

**DEVELOPMENT OF STABLE PVA-PAA-SiO₂
WATER RESPONSIVE SELF-HEALING
MEMBRANE**

GRACE LIM QIAN VON

UNIVERSITI TUNKU ABDUL RAHMAN

**DEVELOPMENT OF STABLE PVA-PAA-SiO₂ WATER RESPONSIVE
SELF-HEALING MEMBRANE**

GRACE LIM QIAN VON


**A project report submitted in partial fulfilment of the
requirements for the award of Bachelor of Chemical
Engineering with Honours**

**Lee Kong Chian Faculty of Engineering and Science
Universiti Tunku Abdul Rahman**

April 2024

DECLARATION

I hereby declare that this project report is based on my original work except for citations and quotations which have been duly acknowledged. I also declare that it has not been previously and concurrently submitted for any other degree or award at UTAR or other institutions.

Signature : 

Name : Grace Lim Qian Von

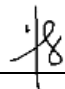
ID No. : 20UEB02782

Date : 29th April 2024

APPROVAL FOR SUBMISSION

I certify that this project report entitled “**DEVELOPMENT OF STABLE PVA-PAA-SiO₂ WATER RESPONSIVE SELF-HEALING MEMBRANE**” was prepared by **GRACE LIM QIAN VON** has met the required standard for submission in partial fulfilment of the requirements for the award of Bachelor of Chemical Engineering with Honours at Universiti Tunku Abdul Rahman.

Approved by,

Signature :  _____

Supervisor : Chong Woon Chan

Date : 29th April 2024

Signature : _____

Co-Supervisor : _____

Date : _____

The copyright of this report belongs to the author under the terms of the copyright Act 1987 as qualified by Intellectual Property Policy of Universiti Tunku Abdul Rahman. Due acknowledgement shall always be made of the use of any material contained in, or derived from, this report.

© 2024, Grace Lim Qian Von. All right reserved.

ACKNOWLEDGEMENTS

I would like to thank everyone who had contributed to the successful completion of this project. I am deeply grateful to my supervisor, Ir. Dr. Chong Woon Chan, whose guidance and expertise were invaluable throughout this research journey. I extend my heartfelt appreciation to the staff of the Department of Laboratory Management and Safety Administration for their assistance during my lab work. I would also like to acknowledge Mr. Wong Eng Cheong and Ms. Koh Yung Xin for their support and advices. Lastly, my sincere thanks to my family for their unwavering encouragement and understanding, without which this research would not have been possible.

ABSTRACT

Water pollution has emerged as a significant environmental issue due to the rising levels of untreated or partially treated wastewater being directly discharged into the river or oceans. Self-healing material that has the ability to localised response to damage in a meantime has come under the spotlight as the alternative means to cope with the issue of declined performance of membrane due to mechanical abrasion. However, the performance and stability of the self-healing membrane still remains a significant challenge. In this present work, PVA-PAA is used as the self-healing material coated on a PES membrane. Silica nanoparticles (SiO_2 NPs) are added to improve the performance of the membrane in terms of water permeation flux, self-healing efficiency, stability in water and mechanical properties. The SiO_2 NPs were synthesized from tetraethyl orthosilicate (TEOS) using the Stöber method and they were characterized using FTIR and XRD. Subsequently, the membranes were prepared by employing six distinct loadings of SiO_2 NPs (0 wt%, 0.1 wt%, 0.2 wt%, 0.3 wt%, 0.4 wt% and 0.5 wt%) in the PVA-PAA composite membranes. Among these modified membranes, the addition of 0.3 wt% SiO_2 NPs showed the most promising results in the PVA-PAA membrane. The PVA-PAA membrane with 0.3% SiO_2 NPs achieved water flux of 53.84 L/m²h and self-healing efficiency of 71.43% and 90.29% after soaking in water for 24 hours and 48 hours, respectively. The dye rejection was 24.87% and 59.13% through the pristine PVA-PAA membrane and 0.3 wt% SiO_2 NPs membrane, respectively. Moreover, the performance of the PVA-PAA membrane containing 0.3 wt% SiO_2 NPs remained stable in terms of water flux and dye rejection even after being submerged in water for 2 weeks. Also, the tensile strength and elongation of the PVA-PAA membrane with 0.3 wt% SiO_2 NPs were measured at 11.41 MPa and 138.73%, respectively, surpassing those of the pristine PVA-PAA membrane. From these findings, it could be concluded that the addition of SiO_2 NPs into the PVA-PAA composite membrane fabrication had greatly contributed to the development of self-healing membrane with enhanced permeability, rejection and stability.

TABLE OF CONTENTS

DECLARATION		i
APPROVAL FOR SUBMISSION		ii
ACKNOWLEDGEMENTS		iv
ABSTRACT		v
TABLE OF CONTENTS		vi
LIST OF TABLES		ix
LIST OF FIGURES		x
LIST OF SYMBOLS / ABBREVIATIONS		xii
CHAPTER		
1	INTRODUCTION	1
1.1	Background of Study	1
1.2	Importance of the Study	4
1.3	Problem Statement	5
1.4	Aim and Objectives	6
1.5	Scope and Limitation of the Study	6
1.6	Outline of the Report	7
2	LITERATURE REVIEW	8
2.1	Membrane Filtration	8
2.1.1	Membrane Filtration Configurations	9
2.1.2	Classification of Membrane Filtration	10
2.1.2.1	Microfiltration	10
2.1.2.2	Ultrafiltration	11
2.1.2.3	Nanofiltration	12
2.1.2.4	Reverse Osmosis	13
2.2	Self-Healing Material	16
2.3	Extrinsic Self-Healing	16
2.4	Intrinsic Self-Healing	18
2.4.1	Non-Covalent Bond	19

2.4.2	Covalent Bond	20
2.5	PVA-PAA as Self-Healing Material	24
2.6	Nanomaterials	26
2.7	Nanoparticles	29
2.7.1	Organic Nanoparticles	29
2.7.2	Inorganic Nanoparticles	30
2.7.2.1	Silver Nanoparticles	30
2.7.2.2	Nanoclay	31
2.7.2.3	Silica Nanoparticles	31
3	METHODOLOGY AND WORK PLAN	37
3.1	Overall Experiment Methodology and Flowchart	37
3.2	List of Materials, Chemicals and Equipment	38
3.2.1	Materials and Chemicals	38
3.2.2	Equipment	39
3.3	Preparation of PVA-PAA Solution	40
3.4	Synthesis of SiO ₂ NPs	40
3.5	Fabrication of PVA-PAA-SiO ₂ Membrane	41
3.6	Characterization of Membrane	41
3.6.1	X-Ray Diffraction (XRD)	42
3.6.2	Fourier-Transform Infrared Spectrometer (FTIR)	42
3.6.3	Scanning Electron Microscope (SEM)	42
3.7	Performance of Membrane	42
3.7.1	Dead-end Filtration System	42
3.7.1.1	Pure Water Flux	43
3.7.1.2	Rejection Test	44
3.7.2	Self-Healing Test	44
3.7.3	Stability Test	45
3.7.4	Mechanical Properties	46
4	RESULTS AND DISCUSSION	47
4.1	Characterization of Membrane	47
4.1.1	X-Ray Diffraction (XRD) Analysis	47
4.1.2	Fourier Transform Infrared (FTIR) Analysis	48

4.1.3	Scanning Electron Microscopy (SEM) Analysis	49
4.2	Performance of Membrane	50
4.2.1	Membrane Permeation Flux	50
4.2.2	Self-Healing Test	52
4.2.3	Membrane Rejection Test	54
4.2.4	Stability Test	56
4.2.5	Mechanical Properties	57
5	CONCLUSIONS AND RECOMMENDATIONS	59
5.1	Conclusions	59
5.2	Recommendations	60
	REFERENCES	61

LIST OF TABLES

Table 2.1:	Classification of Membrane Separation Processes.	15
Table 2.2:	Self-Healing Materials with Different Mechanisms.	22
Table 2.3:	Properties and Application of Different Nanomaterials.	27
Table 2.4:	Different Nanoparticle Based Membrane.	34
Table 3.1:	Materials and Chemicals Used in This Project.	38
Table 3.2:	Equipment Used in This Project.	39
Table 3.3:	Composition of the SiO ₂ NPs respective to the PVA-PAA Solution.	41

LIST OF FIGURES

Figure 1.1:	Reuse of Effluent in Various Applications (Shemer, Wald and Semiat, 2023).	2
Figure 1.2:	Membrane Filtration Market by Region (Precedence Research, 2023).	3
Figure 2.1:	Schematic Diagram of Dead-end Filtration (Huisman, 2000).	9
Figure 2.2:	Schematic Diagram of Crossflow Filtration (Huisman, 2000).	10
Figure 2.3:	Illustration of Nanofiltration Mechanism (Zhang et al., 2023).	12
Figure 2.4:	Mechanism of Reverse Osmosis (Singh, 2006).	13
Figure 2.5:	Mechanism of Extrinsic Self-Healing (Yue, Wang and Zhen, 2022).	17
Figure 2.6:	Microencapsulation Extrinsic Self-Healing Mechanism (White et al., 2001).	18
Figure 2.7:	Mechanism of Intrinsic Self-Healing (Yue, Wang and Zhen, 2022).	19
Figure 2.8:	Diels-Alder Reaction Between Diene and Dienophile (Liu and Chuo, 2013).	21
Figure 2.9:	Schematic Diagram of Thermal Cross-linking between PVA-PAA (Li and Hsieh, 2005).	24
Figure 2.10:	Water Soluble Stability of the PVA-PAA Membrane (a-c) without Crosslinking (d-f) and with Crosslinking (Zhu et al., 2018).	25
Figure 2.11:	Diameter Size of Different Nanomaterials (Agboola et al., 2021).	26
Figure 2.12:	Chemical Structure of Chitosan (Modrzejewska et al., 2009).	30
Figure 2.13:	Chemical Structure of Polystyrene (David Richard Steinmetz, 2007).	30
Figure 2.14:	Structure of the SiO ₂ NPs (Zhuravlev, 2000).	32

Figure 2.15:	Schematic Diagram of Crosslinked PVA-PAA-Si (Song et al., 2014).	33
Figure 3.1:	Overview of the Research Methodology.	37
Figure 3.2:	Dead-end Filtration Cell Unit (Kamal et al., 2019)	43
Figure 3.3:	Introduce Artificial Damage to the Membrane's Surface (Kim, Getachew and Kim, 2017).	45
Figure 4.1:	XRD Patterns for SiO ₂ NPs.	47
Figure 4.2:	FTIR Spectra of (a) SiO ₂ NPs; (b) PVA-PAA Membrane and (c) PVA-PAA-SiO ₂ Membrane.	49
Figure 4.3:	Top-View SEM Images of membrane with (a) pure PVA-PAA; (b) 0.1 wt% SiO ₂ loading; (c) 0.2 wt% SiO ₂ loading; (d) 0.3 wt% SiO ₂ loading; (e) 0.4 wt% SiO ₂ loading and (f) 0.5 wt% SiO ₂ loading.	50
Figure 4.4:	Water Flux of PVA-PAA Membrane with Different SiO ₂ NPs Loading.	51
Figure 4.5:	Self-Healing Efficiency of PVA-PAA Membrane with Different SiO ₂ NPs Loading.	53
Figure 4.6:	Self-Healing Efficiency of PVA-PAA Membrane with Different Healing Period.	53
Figure 4.7:	Top-View SEM Images of SiO ₂ Membrane with (a) Scratch on the Surface and (b) After Immersed in Water for 48 hours.	54
Figure 4.8:	Rejection Performance of Membrane at Different State.	55
Figure 4.9:	Performance of Membrane over Time in terms of (a) Pure Water Flux and (b) Dye Rejection.	57
Figure 4.10:	Stress-Strain Curve of the PVA-PAA Membrane with Different SiO ₂ NPs Loading.	58

LIST OF SYMBOLS / ABBREVIATIONS

J_w	pure water flux, L/m ² h
Q	volume of permeate collected, L
A	effective membrane area, m ²
Δt	permeation time, h
R	rejection of solute, %
C_p	concentration of solute in permeate solution, mg/L
C_f	concentration of solute in feed solution, mg/L
M	weight of the membrane, g
W	rate of weight loss, %
EtOH	absolute ethanol
NH ₄ OH	ammonia hydroxide
UF	ultrafiltration
NPs	nanoparticles
TEOS	tetraethyl orthosilicate
SDG	sustainable development goal
SiO ₂	silica
PVA	polyvinyl alcohol
PAA	polyacrylic acid
FTIR	fourier -transferred infrared spectrometer
PES	polyethersulfone
SEM	scanning electron microscope
RO	reverse osmosis
MF	microfiltration
NF	nanofiltration

CHAPTER 1

INTRODUCTION

1.1 Background of Study

Water covers up to 71 % of the surface of the globe making it one of the essential needs to sustain the ecological processes, human activities and the natural processes. However, with the rapid development of technology and the escalating demands of modern life, water pollution has become a widespread and persistent issue around the world. Recent studies revealed that over two-thirds of the world population are experiencing severe water scarcity which led to illness, desertification, environment degradation and economic impact (Shehata et al., 2023). The major contributors to the water pollution and scarcity are the expansion of population growth, climate changes and the industrial activities. It was found that 50% of wastewater produced by humans is dumped untreated into rivers or oceans, endangering both the environment and human health (Shemer, Wald and Semiat, 2023).

The sustainable development goal (SDG 6) aims to ensure the accessibility of clean water and adequate sanitary facilities through the infrastructure improvement, protection and restoration of water-ecosystem and hygiene education among the public. Water reclamation is the process of recover the useable water from the municipal wastewater and this is crucial to ensure the water security. Although the treated water as known as effluent is not suitable for drinking purposes, it can be widely reused in the industries such as power plants and mills industry, agricultural irrigation and restoration of coastal aquifers. Figure 1.1 portrays the usage of the reclaimed water in different applications around the world (Shemer, Wald and Semiat, 2023).

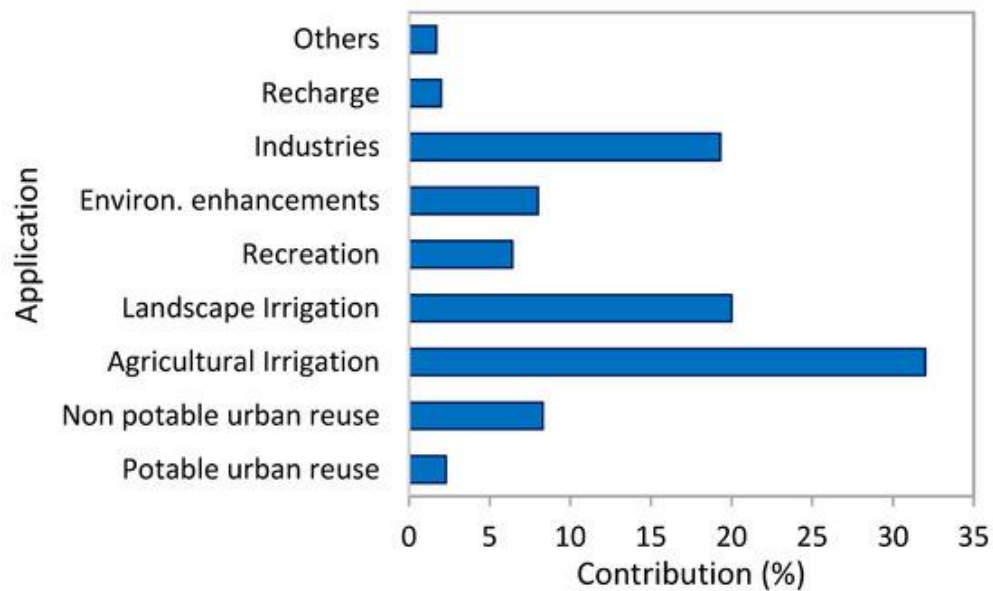


Figure 1.1: Reuse of Effluent in Various Applications (Shemer, Wald and Semiat, 2023).

Dyes is a prevalent type of water pollutant that are non-biodegradable and toxic that possess harm to both the environment and also human health. The release of residual dye from the industrial activities into the aquatic ecosystems constitutes a significant threat to the global environment (Xiao et al., 2021). Tartrazine is one of the dyes that could be found in the effluent from many sectors such as the textile, food and cosmetic industry. Numerous research has highlighted the possible deleterious impact associated with the excessive intake of tartrazine including food allergies, induce of asthma and chronic urticaria (Bouarroudj et al., 2021). Therefore, it is dominant to filter out the dye from the wastewater before discharging the effluent for further usage.

Throughout the pathway in combating with water pollution, the engineers have gain interest towards the membrane technologies which serves the purpose of removing particles and sediments. Research has shown that the membrane filtration market is expected to be dominated by the water and wastewater application segment. Government entities all around the world are promoting membrane filtration technology to supply safe and clean drinking water and household usage as it reduces the use of chemicals in water treatment and offers benefits in terms of effective purification and lower operating cost (Market and Research, 2019). As depicted in Figure 1.2, the usage of membrane

filtration technology is increasing steadily and expected to reach \$38.92 billion by the year 2032 as a result of the expanding population that rise the demand for water needs (Precedence Research, 2023).



Figure 1.2: Membrane Filtration Market by Region (Precedence Research, 2023).

On the other hand, the public has voiced concerns about the controversy surrounding the membrane technology, citing issues such as substantial energy consumption, environmental repercussions and high expenses. Also, decreasing performance of the devices after a long time of operation is a common issue in the industry. To maintain the performance of the device, maintenance or restoration can be made on the failure part. However, replacing the whole module is expensive. Therefore, self-healing material has become a new trend to cope with this issue (Huang and Liu, 2017). This in-situ healing technique helps in minimising waste and increase product longevity. So, it is very crucial to equip the membrane with self-healing capability to lengthen their lifespan.

Polyvinyl alcohol (PVA) is a synthetic polymer that is water soluble, non-toxic and biocompatible to apply in the industry. It was widely studied with the polyacrylic acid (PAA) due to the presence of both hydroxyl group and carboxyl group that could crosslink to form ester bond through thermal esterification (Kononova et al., 2022). This mixed composite membrane

exhibits intrinsic self-healing properties due to the presence of reversible hydrogen bond. In the work of Cordier et al. (2008), the fracture surface of the supramolecular material healed under room temperature when both the fragments are placed close to each other to facilitate the healing process.

Nanoparticles have emerged as promising additives in membrane technology due to their unique properties. The membrane can be enhanced by introducing nanoparticles tailored to improve its performance for particular applications. Nanoparticles offer advantages such as improved mechanical strength, increased hydrophilicity, enhanced selectivity and antimicrobial properties among others. Silica nanoparticles (SiO_2 NPs) has garnered considerable interest among various inorganic materials due to its robust thermal and mechanical stability and established chemical properties (Ngang et al., 2017).

1.2 Importance of the Study

The importance of this study lies in addressing a critical challenge in membrane technology which is the development of self-healing membrane. Self-healing material has been studied due to its various application in the membrane filtration process such as in the textile industry and wastewater treatment. Self-healing technology autonomously identifies material damage and initiates repair processes under specific conditions. Such membranes have the potential to revolutionize various industries by offering longer lifespan, ultimately reducing maintenance costs, environmental impact and reduce downtime.

Besides studies have shown that the incorporation of nanoparticle has the ability to improve the membrane performance in terms of the water permeation flux, dye rejection, self-healing efficiency and enhanced the durability of the membrane. However, limited attention has been given to the utilization of nanoparticles in the fabrication of stable PVA-PAA self-healing membrane. Therefore, this study has accessed the role and performance of the SiO_2 NPs in the self-healing membrane.

1.3 Problem Statement

With the long-term filtration application, damage to membrane is inevitably persist and results in decline performance. This is attributed to the challenge of accurately locating the damaged area, compounded by the fact that prior attempts to develop smart sensors were unsuccessful and incurred high cost. Therefore, there is a burgeoning interest in crafting self-healing materials as a promising solution to address issues related to material degradation and structural damage. Despite advancements in material science, the development of self-healing materials with robust and reliable healing capabilities remains a significant challenge. Previous study done by Lim Yi Heng (2023) with PVA-PAA as self-healing materials showed excellent self-healing ability. However, from our observation, the composite is unstable as it tends to dissolve in water. As a result, the performance of membrane in the wastewater application in long term and results in shorter lifespan of the membrane. Since the stability and mechanical properties of the PVA-PAA self-healing membrane were not investigated in the previous study, nanoparticles were proposed to introduce into the self-healing membrane as it possesses the ability to enhance the performance and stability of the membrane.

This study serves to create a SiO₂ NPs incorporated PVA-PAA self-healing membrane and investigate the performance of the membrane. SiO₂ NPs were selected as it contains large amount of hydroxyl group which enhanced the hydrophilicity of the membrane. Besides, the self-healing efficiency is mainly due to the mobility of free hydroxyl group at the damage site and the formation of hydrogen bonding (Getachew, Kim and Kim, 2017). Lastly, the bonding between the –OH group of SiO₂ NPs with the –COOH group of the PAA molecule is the covalent ester bond which strengthen the bonding between the polymer composite.

1.4 Aim and Objectives

The aim of this project is to fabricate a stable PVA-PAA self-healing membrane by incorporating SiO₂ NPs. The objectives of this project are shown below:

- i. To synthesize and characterize PVA-PAA-SiO₂ polymer composite.
- ii. To investigate the effect of SiO₂ NPs loading on the self-healing efficiency of the PVA-PAA membrane.
- iii. To improve the stability of the membrane with the addition of SiO₂ NPs.

1.5 Scope and Limitation of the Study

The coverage of this study consists of the synthesis of SiO₂ NPs from tetraethyl orthosilicate (TEOS), fabrication of nanoparticles incorporated self-healing membrane and performance investigation. The membrane solution will be thermally treated to form cross-linking between the molecules. After the fabrication of membrane, several tests are carried out to determine the characteristic and performance of the membrane in terms of water permeation flux, rejection, stability and self-healing. X-ray diffraction (XRD) is used to determine the structure of the SiO₂ NPs. The functional group presence in the fabricated membrane will be tested using the fourier transform infrared spectrometer (FTIR) while the morphology of the membrane will be observed through scanning electron microscope (SEM). The water permeation flux and rejection of the membrane will be tested using the dead-end filtration cell unit. Next, the stability of the membrane will be tested in terms of mechanical properties and performance over time. Lastly, the self-healing ability of the membrane will be studied.

There were some limitations encountered during this study. First of all, there were less published study material related to the incorporation of SiO₂ NPs on the PVA-PAA membrane. Therefore, application of SiO₂ NPs on other membrane were referred. Furthermore, the fabricated membrane is in lab scale where the parameter tested might differ significantly from those encountered at an industrial scale. Consequently, this led to the substantial deviations in the performance when transitioning to industrial applications.

1.6 Outline of the Report

In chapter 1, the general introduction related to water pollution and membrane technology is briefly discussed, which include also the importance of study, problem statement, aim of the study and the scope and limitation faced during the project. Next, further studies is done during the literature review in chapter 2. It includes the introduction to membrane filtration such as the filtration methods and the classification of membrane. Moving on, the self-healing mechanism of the membrane and the application of various nanoparticles on the membrane are covered. Chapter 3 outlines the overview of the experiment including the preparation of the SiO₂ NPs, fabrication of membrane, characterization and evaluation on the performance of the membrane. In Chapter 4, the result of the experiment is discussed based on the characterization and performance of the membrane with different SiO₂ NPs loading. Lastly, Chapter 5 conclude the finding of the research project and improvement for further work.

CHAPTER 2

LITERATURE REVIEW

2.1 Membrane Filtration

Filtration is known as the separation technique where solid components are removed from a liquid or gaseous stream (Guillen et al., 2011). The filtration technique has been used in several industries such as water and wastewater treatment, biomedical field, food processing and petroleum. Through the advancement of technology, membrane filtration has now become a widely used technique to retain over undesired species and product that flow through a selectively thin layer of semi-permeable membrane (Asad, Sameoto and Sadrzadeh, 2020). Theoretically, any particles in the feed stream that are larger than the membrane's pore size will be retained on the membrane surface, forming a cake filter while particles that are smaller than the pore size will pass through the membrane resulting in the permeate stream.

The membrane normally acts as a physical barrier between the two homogeneous phases (Singh, 2006). It separates the feed stream into two distinct streams which are permeate and retentate. The effectiveness of membrane filtration depends on the sizes and affinity of the undesired particles to be separated. There are several driving forces facilitate the movement of the feed through the membrane, for instance, using potential gradient in pressure, concentration, temperature or electrical fields (Asad, Sameoto and Sadrzadeh, 2020).

As compared to the conventional filtration methods such as distillation and coagulation which have the disadvantages of high energy consumption and low separation efficiency, membrane filtration is a good alternative to solve these problems. The new membrane technology is more environmentally friendly and economically viable as the physical filtration can be done without the addition of chemical to the feed stream or any phase change (Guillen et al., 2011).

2.1.1 Membrane Filtration Configurations

In general, there are two types of filtration methods which are dead-end filtration and crossflow filtration. It is very important to understand the mechanism of both filtration methods in order to choose the right system for a particular application. These types mostly differ in terms of the flow direction of the feed streams relative to the membrane surface (Asad, Sameoto and Sadrzadeh, 2020).

In the dead-end filtration system, the predominant flow direction of the feed stream and permeate is perpendicular to the membrane surface as depicted in Figure 2.1. The membrane's pores are easily clogged by the particles deposited on the membrane surface when the suspended particles are continuously dragged towards the membrane. When this condition lasts for a long time, the permeate flux will decrease continuously due to the increasing flow resistance caused by the deposition of rejected particles on the membrane surface (Huisman, 2000). Therefore, the membrane used in this system need to undergo maintenance frequently to maintain the optimum performance. However, this system requires a very low capital cost as compared to the crossflow filtration system which will be discussed later.

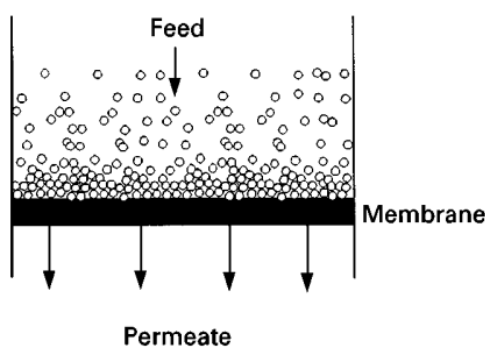


Figure 2.1: Schematic Diagram of Dead-end Filtration (Huisman, 2000).

On the other hand, the crossflow filtration system is more economically friendly due to its built-in mechanism. As seen from Figure 2.2, the feed stream to be filtered is perpendicular to the permeate and it flows tangentially to the membrane surface. The rejected particles that result on the membrane surface are removed by the shear force produced through the interaction between the feed stream and the membrane surface (Asad, Sameoto and Sadrzadeh, 2020). In contrast with the dead-end filtration, crossflow filtration will have one

additional stream which is known as the retentate. The retentate will bring along the larger particles that do not pass through the membrane. This filtration method requires more sophisticated equipment to operate, but it effectively prevents the deposition of particles on the membrane surface. This contributes to the longer lifespan of the membrane, therefore, it is feasible to run a continuous filtration process (Richard W, 2004).

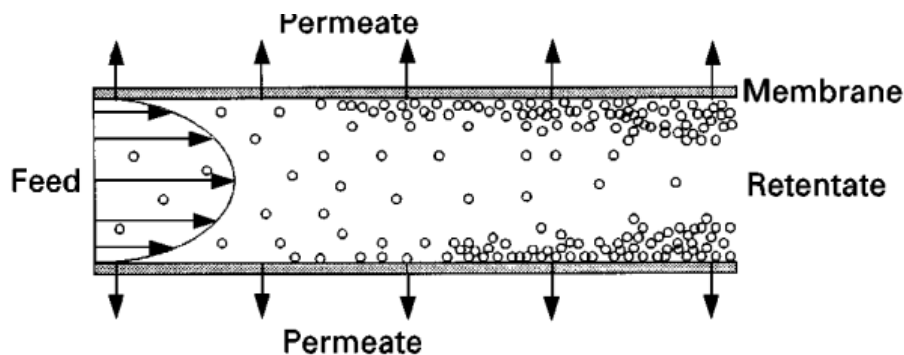


Figure 2.2: Schematic Diagram of Crossflow Filtration (Huisman, 2000).

2.1.2 Classification of Membrane Filtration

Generally, there are few types of industrial membrane technology have been invented and several more are in development. The most common and simplest membrane filtration techniques will be the processes driven by pressure such as microfiltration, ultrafiltration, nanofiltration and reverse osmosis.

2.1.2.1 Microfiltration

Microfiltration (MF) is known as the oldest membrane process used to separate relatively large particles with the size ranging from 0.1 to 10 μm in the feed stream (Ghosh et al., 2015). The separation mechanism is not just a simple sieve mechanism where the larger particles are rejected while the smaller particles flow easily through the pores. In fact, the larger particles adsorbed onto the surface of the membrane reduce the effective pore size of the membrane. Also, the deposition of the rejected particles creates a filter cake which act as a secondary filter layer. Therefore, the particles that MF membrane can separate tend to be smaller than the designed pore size (Singh, 2006).

In general, separation by MF works effectively when the pressure differential is less than 2 bar. It is capable of rejecting particle such as clay and macromolecular-to-cellular size bacteria and fat (Asad et al., 2020). The application of the MF system varies from the bioengineering industry to the wastewater treatment. By utilizing the MF system, bacteria from the fermentation products can be eliminated easily. In addition, some municipalities apply MF to treat the wastewater at the tertiary level (Singh, 2006).

2.1.2.2 Ultrafiltration

Ultrafiltration (UF) is similar to the MF system, but the molecular sieving occurs through progressively smaller pores. UF membranes are denser than MF membranes and it may filter out particles with sizes ranging from 0.01 to 0.1 μm with a driving force of 1-10 bar (Ghosh et al., 2015). For example, it can remove colloids and molecules from the solutions. While UF and MF membranes are both porous by nature, UF membranes have a considerably denser skin layer due to smaller pore size and lower surface porosity, resulting in higher hydrodynamic resistance. Additionally, the UF membrane has an asymmetric structure with the top layer acting as a skin and macropores in the interior. With this structure, the particles have a tendency to flow from a higher-pressure region to the lower pressure region (Singh, 2006).

UF membranes are suitable for usage in a wide range of applications across numerous sectors due to their large pore size range. It can be applied in the industry related to removal of heavy metals from the industrial wastewater, treatment of oil emulsion and pulp and paper industries. One of the most effective large-scale commercial uses of UF is electrodeposition which incorporates with the hollow-fibre membrane to recover the undeposited paint. It is also employed in the beverage sector to raise the product yield and quality. As it aids in removing the microorganism and proteins, the permeate which is the products will have longer shelf life (Singh, 2006).

2.1.2.3 Nanofiltration

Nanofiltration (NF) membranes typically have pores that are smaller than 0.001 μm , which is in the size range between UF and RO which will be discussed in the next part (Ghosh et al., 2015). As the pore size is getting smaller, the NF membrane structure is denser than the UF membrane which lead to increasing of the hydrodynamic resistance. For this reason, NF membrane necessitate a greater driving force which is a pressure ranging from 5-40 bar for filtration (Asad, Sameoto and Sadrzadeh, 2020).

Unlike MF and UF, which separate solutes based on the size, NF technique take into account both charge and size. Due to the ionisable compounds such as carboxylic or sulphonic acid group, the NF membrane has a surface charge. It is often negatively charged due to the ionisable group, therefore, the main factor influencing the rejection of solutes depend on the anion repulsion (Singh, 2006). As illustrated in Figure 2.3, even though the anion particles are smaller than the pore size, the repulsion known as Donnan effect reject the particles from passing through the membrane (Zhang et al., 2023). Consequently, NF membranes are perfectly adapted for rejecting polyvalent ions as well as organics molecule with molecular weights greater than 200 Da such as lactose and sucrose. Application of NF membranes can be widely used in the softening of water and eliminating organic colorants for surface and groundwater sector (Singh, 2006).

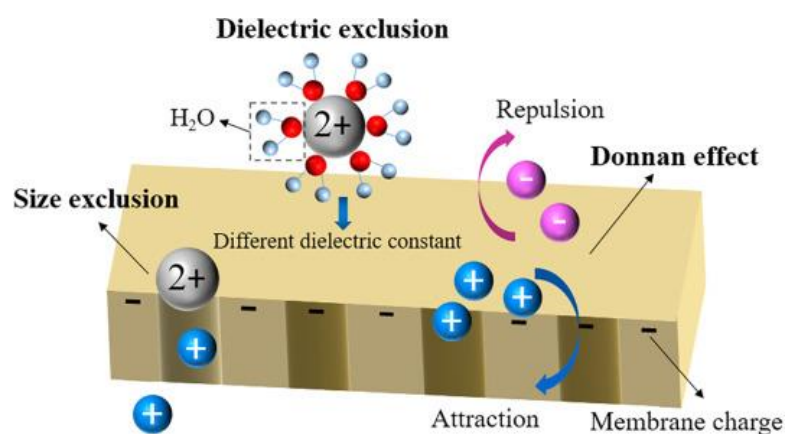


Figure 2.3: Illustration of Nanofiltration Mechanism (Zhang et al., 2023).

2.1.2.4 Reverse Osmosis

Reverse osmosis (RO) is a process where the dissolved solute is removed from the solvent through the semi-permeable membrane. The membrane's pore size is smaller than the other type of pressure driven membrane which is normally in the range of 0.0001-0.001 μm , hence RO membranes are capable of separating small monovalent ions (Asad, Sameoto and Sadrzadeh, 2020). Due to the decreasing pore size of the membrane, higher pressure is needed as compared to the other system. With the operating pressure of 10 to 100 bar, the solvent flows from a high solute concentration zone to a low solute concentration zone (Gürses, Güneş and Şahin, 2021).

When two solutions are placed between the semi-permeable membrane, the solvent from the lower solute concentration solution known as feed will flow to the other side known as permeate. During the equilibrium phase, the osmotic pressure, $\Delta\pi$ needed to prevent the flow of solvent molecules through the semi-permeable membrane is equal to the pressure applied. The natural osmosis mechanism tends to maintain the solute concentration equilibrium of both the feed solution and the permeate (Singh, 2006).

In order to get a highly purified water, pressure greater than the osmotic pressure must be applied on the permeate side and the solvent will eventually be forced out through the membrane against the natural flow motion (Singh, 2006). As a result, the feed stream will be nearly pure solvent and the other will be the low-pressure permeate. This is known as the reverse osmosis, which is the reverse action of the normal osmosis. Figure 2.4 below illustrates the mechanism of RO membrane.

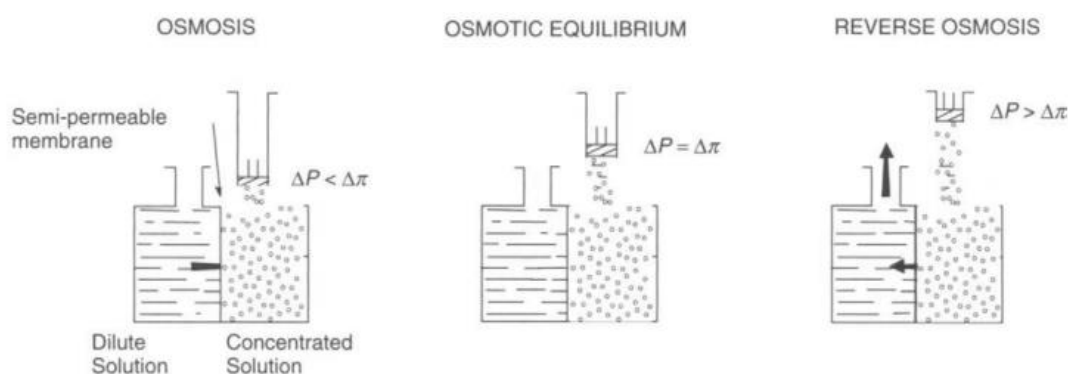


Figure 2.4: Mechanism of Reverse Osmosis (Singh, 2006).

It is often applied in the desalination of seawater or brackish water using membrane that are permeable to water but impermeable to salt. High-quality water can be obtained since it only permits water molecules to pass through meanwhile reject the dissolved potassium, calcium ions and other bacteria (Singh, 2006).

Table 2.1 summarizes the classification of the four different membrane separation processes according to the different aspects such as pore size, driving force, feed and permeate phase, membrane morphology, type of rejections and separation principle.

Table 2.1: Classification of Membrane Separation Processes.

Characteristics	Microfiltration (MF)	Ultrafiltration (UF)	Nanofiltration (NF)	Reverse Osmosis (RO)	References
Pore Size	0.1 to 10 μm	0.01 to 0.1 μm	<0.001 μm	0.0001-0.001 μm	(Ghosh et al., 2015)
Driving Force (Pressure)	< 2 bar	1-10 bar	5-40 bar	10 to 100 bar	(Ghosh et al., 2015)
Feed/Permeate Phase	Liquid/Liquid	Liquid/Liquid	Liquid/Liquid	Liquid/Liquid	(Asad, Sameoto and Sadrzadeh, 2020)
Membrane Morphology	Porous and thin skin layer	Porous, denser skin layer and lower surface porosity	Thin dense top layer and porous sublayer	Thin dense top layer and porous sublayer	(Guillen et al., 2011)
Types of Rejection	Clay, macromolecular-to-cellular size bacteria and fat	Heavy metal, microorganism and proteins	Polyvalent ions	Dissolved potassium, calcium ions and bacteria	(Ghosh et al., 2015; Asad, Sameoto and Sadrzadeh, 2020)
Separation Principle	Size exclusion and sieving	Size exclusion and sieving	Size exclusion and Donnan effect	Solution-diffusion	(Zhang et al., 2023)

2.2 Self-Healing Material

Self-healing material is referred to as the materials that have the ability to regain some or all of their function after experiencing an external damage (Mezzomo et al., 2020). In general, it can be classified into two groups which are extrinsic and intrinsic self-healing. The former occurs when there are embedded with external agent to the system which are not a component of the main polymer network for instance the capsules or vascular system, whereas the latter is based on the healing agent inherent to the material such as reversible bonds under certain external stimuli (Liu et al., 2019a).

The efficiency of self-healing depends on the localization, temporality and mobility of the self-healing agent. Localization refers to the location and the extent of the damage. It can be superficial damage where there are microcracks or cut on the surface; deep damage such as fiber debonding and molecular scale damage. Moving on to temporality, it refers to the time taken for the healing event to occur. It is very crucial to make sure that the healing event take place before the damage become irreversible. In the concept of mobility, the healing agents must diffuse towards the damage region for the self-healing event to take place and the polymer chain movements must encourage the bond reversibility (Utrera-Barrios, et al., 2020).

2.3 Extrinsic Self-Healing

In extrinsic self-healing techniques, the healing agent is encapsulated in the “container” such as the microcapsules, hollow fibres and microvascular network. The healing agent can be made of cross linkable monomers and catalysts, liquid metal alloys or any compound that can aid in healing the damage region (Mezzomo et al., 2020). As depicted in Figure 2.5, the polymer network is embedded with the healing agent. When damage occurred, the encapsulated healing agent will crack and the chemical will leak out and subsequently healing event will occur. It is known as autonomous process.

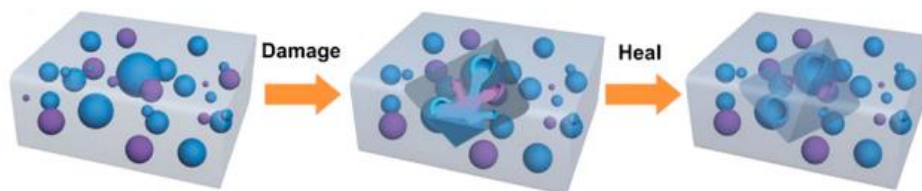


Figure 2.5: Mechanism of Extrinsic Self-Healing (Yue, Wang and Zhen, 2022).

Extrinsic self-healing mechanism is useful as the healing agent could perform instantaneous localised response to damage without any external triggers (Limin and Baghdachi, 2015). Besides, it does not have to modify the chemical properties of the polymer to attain the self-healing characteristics. However, the healing agent incorporated in the polymer during fabrication will be used up as the agent can only provide the reparation once. Therefore, once the healing agent is depleted, the polymer will lose the ability to heal and the damage experienced will be irreversible (Mezzomo et al., 2020).

The concept of microencapsulation self-healing mechanism was first introduced by White, et al. (2001) It was reported that the fabrication of microcapsules was done through the polymerization of urea-formaldehyde (UF) as the shell material. The study was done on an epoxy matrix which also contained Grubbs' catalyst that were mixed with microcapsules containing liquids dicyclopentadiene (DCPD) as the healing agent (Figure 2.6a). When a microcrack developed in the matrix, it tends to expand and penetrate through the microcapsules results in the discharge of liquid DCPD to fill up the cracked damage area (Figure 2.6b). Ring-opening metathesis polymerization (ROMP) process was triggered whenever the DCPD reacted with the Grubbs' catalyst forming a cross-linked network (Figure 2.6c) (White et al., 2001).

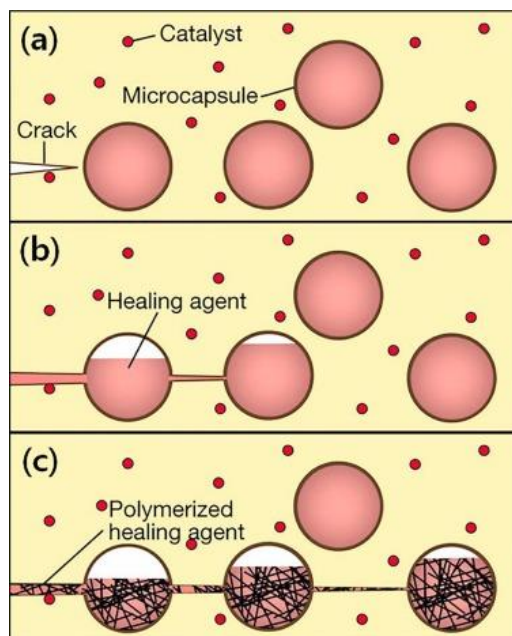


Figure 2.6: Microencapsulation Extrinsic Self-Healing Mechanism (White et al., 2001).

2.4 Intrinsic Self-Healing

Another concept was intrinsic self-healing which depends on the chemistry of the dynamic bonds. Dynamic bond can be categorised into two groups which are covalent and non-covalent bond that are reversible under equilibrium conditions (Utrera-Barrios et al., 2020). Due to its reversible properties, the material can be repaired after damaged. The material is designed through functionalizing the interacting group between the polymer to perform the reversible healing process (Mezzomo et al., 2020). In contrast with the extrinsic method, intrinsic self-healing mechanism is more stable as it does not have to encapsulate the healing agent into the matrix. As a result, intrinsic self-healing does not have the issue of depletion of healing agent and it is capable for multiple recoveries (Yue, Wang and Zhen, 2022).

On the other side, intrinsic self-healing mechanism has its drawbacks too. The healing process is relatively slower than the extrinsic method due to its slow kinetic bond reorganization. Besides, material recovery efficiency is highly dependent on the mobility of the reversible iterative reformation of the bond (Mezzomo et al., 2020). Therefore, it is very important to determine the functional group of the polymer matrix to ensure that reformation of bond between the functional group is applicable.

The mechanism of intrinsic self-healing is better explained with Figure 2.7. As the healing agent is in the form of function group within the polymer matrix, healing event will not be activated spontaneously when the damage happens to the polymer matrix. Unlike extrinsic method, the healing process of intrinsic method normally need an addition external stimulus such as heat, light, water or pH. These stimuli will trigger the reversible healing event to happen (Yue, Wang and Zhen, 2022).

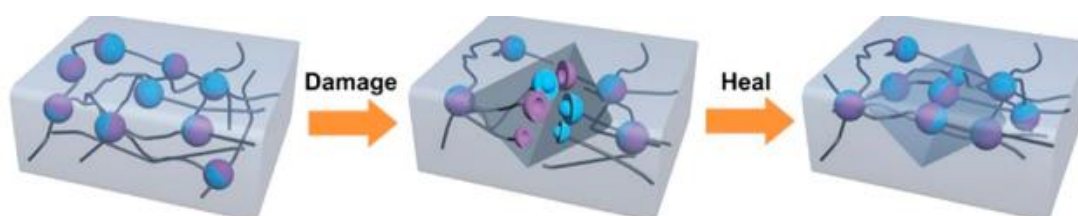


Figure 2.7: Mechanism of Intrinsic Self-Healing (Yue, Wang and Zhen, 2022).

2.4.1 Non-Covalent Bond

The non-covalent bond refers to the intermolecular forces between molecules without the sharing of electron pairs. For example, the metal-ligand coordination, π - π stacking interactions and the most widely applied mechanism is the hydrogen bond. Less energy is required for the formation and breaking of non-covalent bond, therefore this bonding is weaker. In addition, due to its low energy requirement, the application of these non-covalent reversible bond is highly susceptible to the environment where diffusion of the healing agent can be effective even in room temperature. This contributes to the reversibility of the process as the damaged bond can easily and spontaneously reformed without any external intervention (Mezzomo et al., 2020).

The bond strength of the hydrogen bond can be ranged from 2 to 40 kcal/mol, depending on the characteristics of the donor and acceptor involved. Its interaction is between the hydrogen atom and the high electronegativity atoms like nitrogen and fluoride atoms. In the work of Xu et al. (2019), they have reported a self-healing epoxidized natural rubber incorporated carboxymethyl chitosan (ENR/CMCS) composites through the hydrogen bonding of multiple hydrophilic groups of unfolded CMCS molecules to the ENR molecules. The tensile strengths of the ENR with 5 and 10 wt% CMCS

were found to be 1.40 and 1.92 MPa, respectively. In additionally, the self-healing efficiency of both composites reached 90% after 12 hours at room temperature. On the other hand, it was also noticed that with the addition of CMCS exceeding 10 wt%, there was increased in the mechanical strength of the composite but decreased effect on the self-healing efficiency due to the unavoidable agglomeration of the CMCS filler.

2.4.2 Covalent Bond

It was mentioned in last Section 2.4.1 that non-covalent bonds are weak and unstable. Conversely, covalent bonds often have a higher bond energy, allowing the material to have satisfactory mechanical properties and the capacity to heal itself. Due to this fact, the covalent based self-healing material requires an external stimulus as the energy needed to form bonds is greater than the thermal energy present at ambient temperature (Mezzomo et al., 2020). The self-healing efficiency of the associated polymer can be optimized by altering the types of reversible dynamic bonds and the mobility of the chain. It must also take into consideration that the degree of damage. For instance, the interfaces of damaged positions need to be sufficiently close to one another at the macroscopic level to support the dynamic reorganisation process; in molecular level, the resulting polymers must offer a large number of dynamic interactions to provide sufficient dynamics of the polymer chain (Yue, Wang and Zhen, 2022).

There are few a fabrication approaches for intrinsic covalent self-healing polymer while the best-known approach will be the Diels-Alder. Diels-Alder (DA) reaction is a thermally reversible reaction which is desirable to design for a heat responsive self-healing polymer. The reversed action of DA reaction is known as the retro-DA reaction where during high temperature, the respective functional groups were prone to regenerate and reforming bond upon cooling. The DA reaction is a cycloaddition between a diene and a dienophile with electron-withdrawing group where the bond formed is thermally unstable. Taking furan-maleimide groups into the discussion, maleimide group has two C=O bonds which are electron-withdrawing group that made the maleimide group electron insufficient and more reactive to the diene group which is furan in this case as shown in Figure 2.8. However, with a simple DA reaction between one furan and one maleimide exhibited comparatively poor chain

mobility which limit the polymer from self-healing application (Liu and Chuo, 2013).

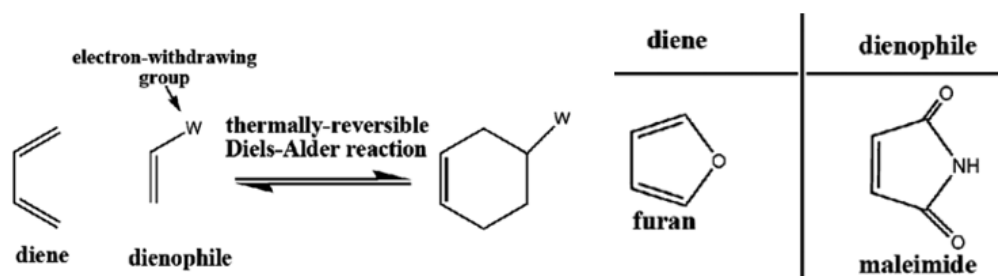


Figure 2.8: Diels-Alder Reaction Between Diene and Dienophile (Liu and Chuo, 2013).

Further modification has been made on the furan-maleimide group to have better self-healing efficiency through DA reaction. As reported by Chen, et al. (2002), multi-furan (F) and multi-maleimide (M) were used to form a highly cross-linked polymer known as 3M4F. The research showed that in the polymer network of 3M4F, the retro-DA reaction was more preferable than bond-breaking degradation event when heat was induced to it. With the healing temperature between 120 to 150 °C, it was observed that the self-healing efficiency could reach about 41% and 50%, respectively. This showed that the thermal sensitive polymer projected better self-healing effect during high temperature. Also, several healing cycles were tested during the experiment, proving that the DA reaction between furan-maleimide group were applicable for multiple healing cycle with a recovery of 80% (Chen et al., 2002).

Table 2.2 below summarizes the self-healing material at different mechanisms while the results of self-healing efficiency are discussed.

Table 2.2: Self-Healing Materials with Different Mechanisms.

Mechanism	Self-Healing Material	Results	Reference
Hydrogen Bond	BPVA-Pluronic in Microcapacitor	Hydrogen bonds were form between the BPVA chains and Pluronic chains; BPVA-Pluronic-5 hydrogel exhibited self healing efficiency of 96.29% in 1 hour without any external environment stimulation; In the application of microcapacitor, the BPVA-Pluronic shown an excellent capacitance retention of 90.43% after 5 breaking/self-healing cycles with an initial reading of 97.59%.	(Wang et al., 2021)
	PVA, Succinic anhydride, Dopamine	Hydroxyl group of PVA engaged with dopamine thourgh the catechol and amine functional groups at the interface, facilitating the regenration of hydorgen bonding network; Healing efficiency increased with dopamine content due to increased molecular chain mobility.	(Li and Xia, 2017)

Table 2.2: Continued.

Diels-Alder	HBSR, α,ω -aminopropyl polydimethylsiloxane, ethylene carbonate	Hydrogen bonded between carbonyl and imino groups; Thermal induced self-healing; Healing efficiency increased from 73.1% to 88.5% with the healing temperature of 40°C and 80°C, respectively.	(Liu et al., 2019b)
	Fulvene-modified Dextran and Dichloromaleic-acid-modified Poly(ethylene glycol)	DA bonded between the functional group of PEG–DiCMA (dichloromaleic acid groups) to Dex-FE (fulvene group); Healing efficiency increased from 24.6% to 98.7% with the healing time increased from 2 h to 7 h without external stimuli.	(Wei et al., 2013)
	Cellulose nanocrystal-Poly(ethylene glycol)	Reversible DA bonds formed through furyl groups attached to CNC and malamide groups in PEG; Healing efficiency increased from 35% to 78% with the healing time increased from 1 hr to 24 h.	(Shao et al., 2017)

2.5 PVA-PAA as Self-Healing Material

Polyvinyl alcohol (PVA) is one of the polymers that have been widely studied for its self-healing properties. PVA is a semi-crystalline synthetic polymer having multiple features such as nontoxic properties, biodegradable and biocompatible. It functions well as a barrier against oxygen and aromatics and is impermeable to solvents and oils. However, due to the presence of hydroxyl group (-OH), the polymer is highly hydrophilic. Therefore, PVA tends to have poor moisture stability which leads to weaken barrier characteristics and plasticization. With this, the PVA polymer tends to dissolve when get in contact with water (Spoljaric et al., 2014).

Researchers started to study on the methods to enhance the insolubility of PVA through crosslinking. In recent studies, polyacrylic acid (PAA) has shown promising results and gained popularity as the crosslinking agent for PVA polymer in both biomedical and separation membrane application due to its high miscibility with PVA (Paralikar, Simonsen and Lombardi, 2008). PAA has a functional carboxyl group (-COOH) that could bind with the hydroxyl group of the PVA. The crosslinked PVA-PAA membranes through applying heat can be employed as heavy metal adsorbent in the wastewater industry (Kim et al., 2019).

The idea of introducing PAA into the PVA polymer is to increase the physical crosslinking through the heat induced esterification process. Figure 2.9 shows the strong ester linkage formed between the carboxyl group of the PAA and hydroxyl group of PVA. As a result, the membrane has effective crosslinking and enhanced resistance to barriers. The self-healing ability is achieved when the free hydroxyl group remained on the scratched interfaced formed multiple reversible hydrogen bond due to the availability of sufficient molecular chain mobility (Jucius, Lazauskas and Gudaitis, 2019).

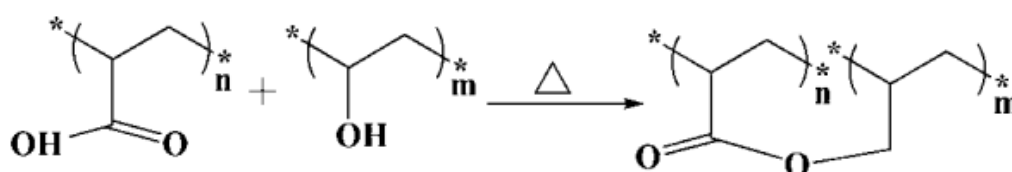


Figure 2.9: Schematic Diagram of Thermal Cross-linking between PVA-PAA (Li and Hsieh, 2005).

In Kim et al. (2019) work, they have successfully proven through experiment that by crosslinking hydroxyl and carboxyl groups with heat treatment at 160 °C for 1 hour, the PVA-PAA water-soluble nanofibers became insoluble. This is also proven in the study of Zhu et al. (2018) that the solubility of PVA-PAA decreased upon the thermal crosslinked treatment at 140 °C for 2 hours. As illustrated in Figure 2.10, when the PVA-PAA nanofibers membrane prior to thermal treatment was submerged in water (a-c), it disintegrated instantly while the crosslinked PVA-PAA membrane remained durable throughout the experiment (d-f) (Zhu et al., 2018).

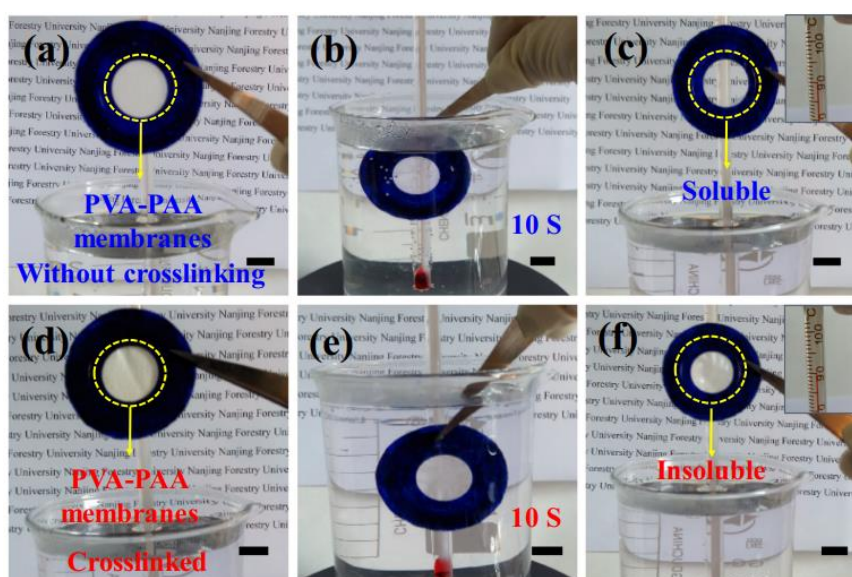


Figure 2.10: Water Soluble Stability of the PVA-PAA Membrane (a-c) without Crosslinking (d-f) and with Crosslinking (Zhu et al., 2018).

Besides, Wu et al. (2020) reported that the PVA-PAA film has higher elastic modulus proving that the double-network formed increased the mechanical strength of the hydrogel film. According to Chen & Zhang (2010), they found that the PVA-PAA solution with lower concentration, 6 wt%, dissociated easily during shearing as the space between molecular was bigger than in the high concentration solution which was 12 wt%. As a result, the strong interactions between molecular chains were less likely to develop. In addition, the presence of PAA improved the mechanical properties of the film with a

tensile strength increased from 89.31 MPa to 119.8 MPa for the blending ratio of PVA-PAA from 100:0 to 60:40, respectively.

2.6 Nanomaterials

Nanotechnology has been widely studied on the polymer network due to their potential ability to have a positive effect on the mechanical strength of the polymer as well as some of the unique functions such as enhance metal adsorption, electronic conductivity and magnetic response. There are different variety of nanomaterials with the size ranging from 1-100 nm that were utilized in the fabrication of nanocomposite polymer as shown in Figure 2.11. Due to the alteration of the material's size and the momentum gained at the surface of the material's atom, the exhibited properties and functions are distinctive and enhance the utilization of polymer in the environment (Agboola et al., 2021). The different properties possess in the nanomaterials are discussed in Table 2.3.

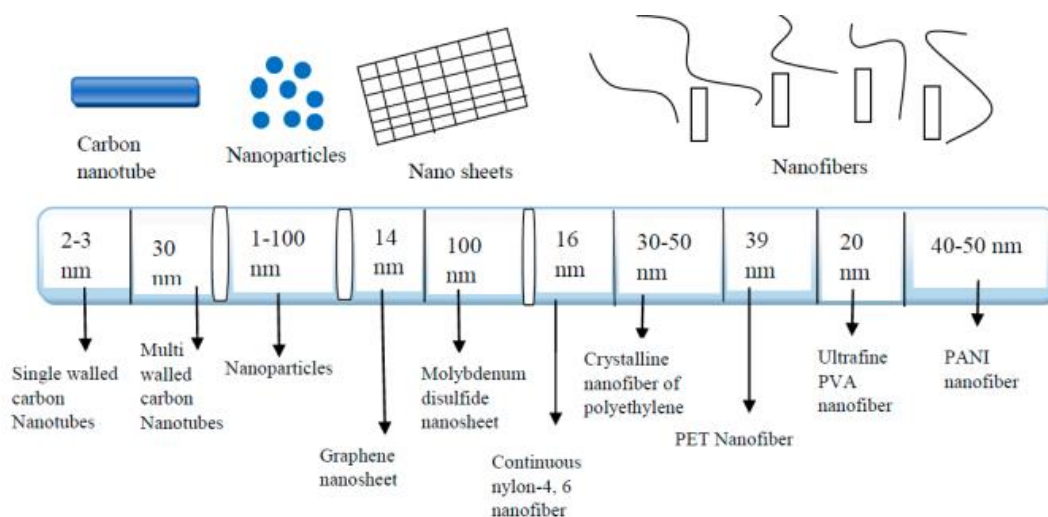


Figure 2.11: Diameter Size of Different Nanomaterials (Agboola et al., 2021).

Table 2.3: Properties and Application of Different Nanomaterials.

Nanomaterials	Properties	Application	References
Carbon Nanotube	High thermal and electrical conductivity; Selectivity towards aromatics; Large length to diameter ratio with diameter smaller than 2.5 nm but macroscopic length; High adsorption efficiencies due to its large surface area and abundant porous structure; High tensile strength due to its C-C bond Well defined adsorption sites.	Sorption processes; Drug delivery in tissue engineering; Removal of heavy metal in wastewater.	(Lu et al., 2016; Agboola et al., 2021; Findik, 2021)
Nanoparticles	High surface to mass ratio; Size dependent optical properties, reactivity and toughness; Characterised by high particle mobility High association between atom and surface.	Photodegradation; Removing of heavy metal in wastewater; Act as sensor to detect pathogen in wastewater; Use in coating, lubricant and adhesive applications; Gas separation.	(Khan, Saeed and Khan, 2019; Agboola et al., 2021)

Table 2.3: Continued.

Nanosheet	High thermal and electrical conductivity; Large surface area advantageous for the creation of polymeric composites; Possess large quantity of active oxygen-containing groups.	Cell differentiation and tissue regeneration; Pervaporation application.	(Suhas et al., 2015; Agboola et al., 2021)
Nanofibers	Large surface area and high aspect ratio with improved surface properties; Extreme adsorption capacity; Large number of pores and small pore size, suitable in filtration applications.	Drug delivery in tissue engineering; Applied in photovoltaic panels and rechargeable batteries; Sensor application.	(Agboola et al., 2021)

2.7 Nanoparticles

In recent years, the integration of nanoparticles into membranes has become an interesting topic fuelled by the advantageous such as increase in the selectivity, water permeation flux and mechanical stability based on the size and selected nanoparticles. Nanoparticles are added to the membrane during fabrication in order to fill the membrane composites to improve the interaction between the two phases of the membrane (Khraisheh et al., 2021).

In general, nanoparticles serve as the multifunctional cross-linkers for the membrane where two or more polymer chains will bind to one of the nanoparticles and the other end of the polymer chain binds to another nanoparticles, results in a nanocomposite membrane. The degree of interaction between the polymer monomers and the nanoparticle surface does not necessitate a significant magnitude. Due to its conformational entropy and consequent ability to adopt various structure, the polymers are able to form strong interaction multiple links to prevent the network from dissolve when exposed to excess water (Dannert, Stokke and Dias, 2019).

Moreover, certain polymers will detach from the nanoparticles to alleviate the tension and slow down failure of the membrane when it experiences tension. At the meantime, the disrupted cross-linking can be repaired as the adjacent strand can subsequently bind to the nanoparticles replacing the detached link. This mechanism demonstrates how the nanocomposite membrane exhibits self-healing ability (Dannert, Stokke and Dias, 2019).

2.7.1 Organic Nanoparticles

Nanoparticles can be classified into two categories which are organic and inorganic nanoparticles depending on their composition. Organic nanoparticles refer to the carbon-based molecules which are biodegradable and non-toxic in nature. For example, chitosan is utilized in varies fields including biomedical, pesticide and water treatment industries. Its excellent adsorbent features aid in the treatment of wastewater by eliminating hazardous contaminants involving metal ions, dyes and proteins (Nakum and Bhattacharya, 2022). Apart from that, the polystyrene function as the crosslinker that engage with initiator molecules to perform in situ free radical polymerization on their surface (Xing and Tang,

2022). Figure 2.12 and Figure 2.13 illustrates the structure of the chitosan and polystyrene, respectively with carbon molecules.

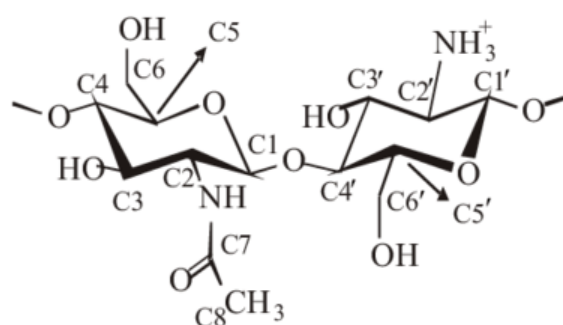


Figure 2.12: Chemical Structure of Chitosan (Modrzejewska et al., 2009).

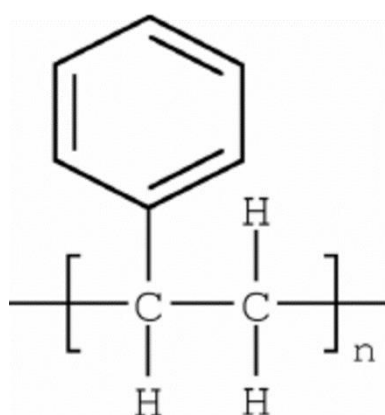


Figure 2.13: Chemical Structure of Polystyrene (David Richard Steinmetz, 2007).

2.7.2 Inorganic Nanoparticles

Nanoparticles formed of non-carbon based compounds are known as inorganic nanoparticles which are comparatively toxic than organic nanoparticles due to the addition of heavy metals or other compounds such as clay and silica.

2.7.2.1 Silver Nanoparticles

Silver nanoparticles (Ag NP) is one of the metal nanoparticles that significantly improve the mechanical properties of the membrane through the interaction between the polymer chain and the nanoparticles (Xing and Tang, 2022). In biotechnology and medicine field, Ag NP is frequently applied as they exhibit antimicrobial properties such as cytotoxicity but relatively low toxicity to

human cell (Nadtoka et al., 2020). Furthermore, Ag NP incorporated membrane shows antibiofouling effect that could cope with biofouling which is considered as one of the barrier in the use of membrane technology. As organisms are capable of self-replication, biofouling is significantly more challenging to remove as compared to organic fouling. In general, biofouling can be controlled through anti-adhesion of the bacterial adsorption to the membrane and anti-bacterial to reduce the activity of attached organisms (Huang et al., 2016). Nevertheless, uniform dispersion of metal-based nanoparticles in a membrane is hard to be achieved through chemically alteration. Thus, in situ synthesis of the nanoparticles in the membrane has been recommended to reduce the aggregation of nanoparticles (Xing and Tang, 2022).

2.7.2.2 Nanoclay

Anisotropic, plate-like, stiff nanoclays are normally serve as reversible multifunctional crosslinkers that exhibit higher mechanical strength and toughen membrane. Strong interactions between the polymer chain of the membrane composite and nanoclays are developed through adsorption and desorption, therefore, nanoclays exhibit good adsorption ability (Xing and Tang, 2022). There are few types of nanoclay that commonly used in the membrane composite such as laponite and MMT clay. Laponite nanodiscs are synthetic silicate clay that show extremely hydrophilic properties. Due to their substantial surface area, biocompatibility and significant cationic exchange capacity, laponite has been known as promising nanofiller in the biochemistry, medical and pharmaceutical industries (Selim et al., 2020). In addition, montmorillonite (MMT) clay has been recognized to improve the thermal stability and degradation performance of the polymer matrices. It is also widely utilized to offer improved mechanical strength and barrier characteristics (Spoljaric et al., 2014).

2.7.2.3 Silica Nanoparticles

Silica nanoparticles (SiO_2 NPs) are widely employed among inorganic nanoparticles due to their relectively low cost and superior physical characteristics such as easily controlled size, posses uniform structure and low (Boonmahitthisud et al., 2017). Moreover, the incorporation of SiO_2 NPs into

the composite membrane demonstrates appealing thermal and chemical stability (Lin et al., 2012). It was observed that the surface of the SiO₂ NPs are surrounded by the hydroxyl (silanol) group, ≡Si–OH as illustrate in Figure 2.14 (Zhuravlev, 2000). Hence, the inclusion of SiO₂ within the membrane composite enhances the membrane surface's hydrophilicity.

Additionally, the SiO₂ NPs carry a negative charge which contributes to further improving the membrane's rejection performance (Lin et al., 2012). Furthermore, the porosity of SiO₂ NPs greatly affect the performance of the membrane in the aspect of water permeation flux and rejection. It has been observed that SiO₂ NPs augment the water permeation flux of mixed matrix membranes while maintaining their selectivity. This is attributed to the strong compatibility between SiO₂ NPs and the polymer matrix.

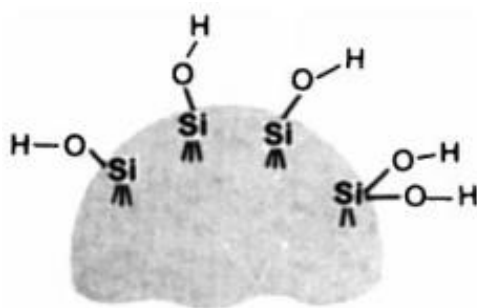


Figure 2.14: Structure of the SiO₂ NPs (Zhuravlev, 2000).

When the SiO₂ NPs are introduced into the PVA-PAA polymer network, the –OH groups of the SiO₂ NPs forms the covalent ester bond with the –COOH group of the PAA molecule while another –OH groups of the SiO₂ NPs will form hydrogen bond with the –OH groups of PVA molecule. The formation of ester bond strengthen the tensile strength of the membrane. Also, the –OH groups presence on the SiO₂ NPs surface increased the hydrophilicity of the polymer matrix (Xu et al., 2022). The schematic diagram for the crosslinked PVA-PAA-Si is shown in Figure 2.15.

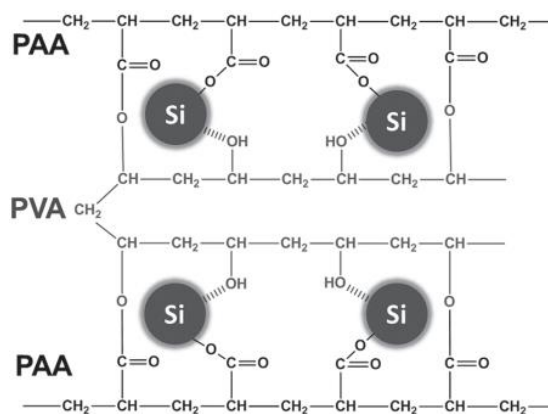


Figure 2.15: Schematic Diagram of Crosslinked PVA-PAA-Si (Song et al., 2014).

In the work of Kim, et al. (2019), the results obtained shown that with the addition of thiol-modified SiO_2 NPs, the swelling characteristics of the membrane can be altered. The swelling ratio of the PVA-PAA membrane has enhanced from 8.703 to 18.20. The extent of swelling is one of the factors that affect the self-healing efficiency of the membrane. Membrane that exhibits higher degree of swelling demonstrated superior self-healing efficiency (Getachew, Kim and Kim, 2017). In addition, the effect of PVA-PAA-Si nanocomposite membrane was studied by Zhu, et al. (2018). Higher tensile strength had been examined through the addition of 4 wt% SiO_2 NPs with an increase of 3.54 MPa. However, the water permeation flux and rejection of SiO_2 NPs incorporated in PVA-PAA membrane has not been studied yet.

Table 2.4 below shows the application of selected nanoparticle in different mambrane application and its enhancement towards the membrane.

Table 2.4: Different Nanoparticle Based Membrane.

Nanoparticle	Membrane Application	Enhancement	Reference
Ag	PDA-PSf-Ag	Improved pure water flux from 248 to 336 L/m ² h; Improved BSA rejection from 78% to 84%	(Huang et al., 2016)
	TFC-Ag	Improved pure water flux from 13.24 ± 1.44 L/m ² h to 17.41 ± 0.69 L/m ² h; Slight influenced on Na ₂ SO ₄ rejection from 86.89 ± 2.10% to 86.15 ± 5.48%	(Liu et al., 2015)
	PA-PSf-Ag	Slightly increase in salt rejection from 89% to 91.7%; Enhanced permeate flux from 16.5 L/m ² h to 32 L/m ² h with the AgNP concentration increased from 0 to 0.3 wt%	(Shawky et al., 2020)
	TFC-S-Ag	Incerased pure water flux from 67.1 L/m ² h to 88.7 L/m ² h; Slightly decreased in NaCl rejection from 95.9 ± 0.6% to 93.6 ± 0.2%	(Yin et al., 2013)

Table 2.4: Continued.

Nanoclay	PA-CS-15A	Improved water flux from 15 L/m ² h to 18.65 L/m ² h; Improved salt rejection from 72% to 80%	(Zaidi et al., 2019)
	PA-MMT	Improved water flux from 15 L/m ² h to 40 L/m ² h; Remarkable reduction in rejection from 70% to 23%	(Zaidi et al., 2019)
	PVA-PAA-NFC-MMT	Enhanced young's modulus and break strength;	(Spoljaric et al., 2014)
	PNIPA-Laponite	Improved mechanic strength from 27 kPa to 69 kPa	(Haraguchi, Takehisa and Fan, 2002)
	PVA-Laponite	Increased in swelling properties with the addition of 2 wt% laponite and decreased with further addition of laponite; Increased water permeation flux from 20.25 kg/m ² h to 34.1 kg/m ² h with 2 wt% of laponite;	(Selim et al., 2020)

Table 2.4: Continued.

SiO ₂	PVA-nano Si	Decreased in contact angle from $78 \pm 1^\circ$ to $45 \pm 1^\circ$ with 69.9 wt% of nano silica; Permeability improved sharply with addition of nano silica from 0 to 50 wt% and the permeability declined as the nano silica exceed 50 wt%; Separation factor initially rose with the inclusion of 29.9 wt% of nano silica, but decreased with further addition of nano silica.	(Lin et al., 2012)
	Cellulose based-Si	Improved tensile strength from 840 ± 55 kPa to 1720 ± 84 kPa with 6 wt% of silica and further addition of silica lead to reduction in tensile strength; Enhanced elastic properties.	(Boonmahitthisud et al., 2017)
	PVA-PAA-nano Si	Tensile strength improved from 5.2 MPa to 8.74 Mpa with with 4 wt% of silica.	(Zhu et al., 2018)
	PSf-CDs-SiO ₂	Water permeation flux increase from 3.51 L/m ² h to 7.4 L/m ² h with 1wt% of CD-SiO ₂ ; Dye rejection increased from 14.52% to 50.54% with 2.5 wt% of CD-SiO ₂ .	(Heng et al., 2021)

CHAPTER 3

METHODOLOGY AND WORK PLAN

3.1 Overall Experiment Methodology and Flowchart

Figure 3.1 depicts the overall flow of the development of PVA-PAA-SiO₂ membrane. This study started from the fabrication of stable self-healing membrane by incorporating different loading of self-synthesize SiO₂ NP into the PVA-PAA solution. Next, the characterization of membrane was investigated using FTIR analysis and SEM analysis. Lastly, the performance of membrane namely pure water flux, dye rejection, stability and self-healing ability were determined.

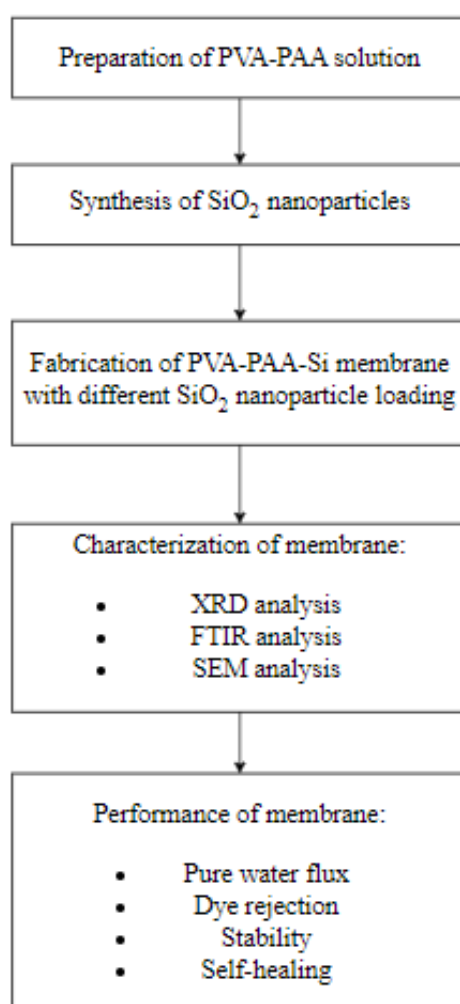


Figure 3.1: Overview of the Research Methodology.

3.2 List of Materials, Chemicals and Equipment

Various types of materials and chemicals were required for the fabrication of self-healing membrane and different types of equipment were used to evaluate the characteristic and performance of the membrane. The materials and chemicals are listed in Section 3.2.1 and the equipment are listed in Section 3.2.2.

3.2.1 Materials and Chemicals

Table 3.1 presents a summary of materials and chemicals used in this project together with their respective specifications.

Table 3.1: Materials and Chemicals Used in This Project.

No	Chemical	Purity (%)	Supplier	Purpose of Use
1	Polyvinyl alcohol (PVA)	87-90	Sigma-Aldrich	Act as the coating mixture.
2	Polyacrylic acid (PAA)	35	Sigma-Aldrich	Act as the coating mixture.
3	Polyethersulfone (PES)	-	Rising Sun Membrane Technology Co., Ltd.	Membrane polymer.
4	Distilled water	-	-	Act as solvent for the synthesis of SiO ₂ NPs; Used as the feed solution in pure water flux test; Use in the stability test; Use in self-healing process.
5	Tartrazine dye	≥ 85	Sigma Aldrich	Used as the feed solution in dye rejection.

Table 3.1: Continued.

6	Tetraethyl orthosilicate (TEOS)	98	Sigma Aldrich	Act as the silica source for the synthesis of SiO ₂ NPs.
7	Absolute ethanol (EtOH)	99.9	Fluka	Act as solvent for the synthesis of SiO ₂ NPs.
8	Ammonium hydroxide (NH ₄ OH)	28	Sigma Aldrich	Act as catalyst for the synthesise of SiO ₂ NPs.

3.2.2 Equipment

Table 3.2 presents a summary of equipments used in this project together with their function.

Table 3.2: Equipment Used in This Project.

No	Equipment	Purpose of Use
1	Hot Plate	To heat the solution.
2	UV-Vis Spectrophotometer	To determine the concentration of the solution.
3	Scanning Electron Microscope (SEM)	To analyse the surface morphology of the membrane.
4	Dead-end Filtration Cell Unit	To test the water permeation flux and rejection of the membrane.
5	Oven	To dry the membrane and use for thermal cross-linking.
6	Fourier Transform Infrared Spectrometer (FTIR)	To determine the functional group in the membrane.
7	Magnetic Stirrer with Magnetic Stir Bar	To stir and obtain homogenous mixture.
8	Tensile Tester	To assess the tensile strength and elongation at break of PVA-PAA-SiO ₂ membrane.
9	X-Ray Diffractor	To determine the structure of SiO ₂ NPs.

Table 3.2: Continued.

10	Centrifuge	To separate the SiO ₂ NPs with the solvent.
----	------------	--

3.3 Preparation of PVA-PAA Solution

The PVA beads was first dissolved in distilled water and stirred magnetically at 300 rpm and 80 °C for 6 hours using hot plate to obtain 5 wt% of PVA solution. An equal weight percentage of PAA solution was prepared by diluting the 35 wt% PAA to 5 wt% using distilled water. The PVA-PAA mixture with molar ratio of 3:1 was prepared with 75 ml of PVA mixing with 25 ml of PAA at 60 °C for 1 hour to form a homogenous solution.

3.4 Synthesis of SiO₂ NPs

Based on the Stöber method, SiO₂ NPs were synthesized from the tetraethyl orthosilicate (TEOS) through sol-gel process. The TEOS act as the silica, while water and absolute ethanol function as the solvents. Ammonia solution (NH₄OH) acted as catalyst that initiate the reaction. The Stöber method involves two reactions which are hydrolysis of TEOS to form silicic acid and formation of silica with siloxane bridges through condensation (M. Ways et al., 2020).

Firstly, 3.35 mL of 0.015 mol of TEOS was hydrolysed by 14.5 mL of 0.5 mol of EtOH and stirred for 5 mins in room temperature. Next, 2.27 mL of 0.12 mol of NH₄OH, 0.5 mL of 0.03 mol of water and 14 mL of 0.5 mol of EtOH were added into the solution where the condensation happened. The solution was continuously stirred at 300 rpm for 6 hours at room temperature for complete reaction. The resulted white turbid solution was centrifuged for 10 mins at 10,000 rpm and dried in oven for 2 hours at 140 °C to obtain the solid powder (Burcu Altin, 2009).

3.5 Fabrication of PVA-PAA-SiO₂ Membrane

The synthesized SiO₂ NPs were added into the PVA-PAA solution and stirred at 100 rpm at room temperature for 1 day. Different loading of the SiO₂ NPs was added into the PVA-PAA solution following the composition shown in Table 3.3.

The commercial PES membrane was cut into a 5.1 cm diameter circle and cleaned using distilled water followed by drying in room temperature. The homogenous casting solution was then slowly poured onto the pre-cleaned and dried PES membrane. Next, the coated membrane was dried in vacuum oven at 35 °C, 0.4 bar for 30 minutes to remove excess ethanol and pure water. Lastly, the coated membrane was heated to catalyse crosslinking between PVA-PAA at 140 °C for 5 minutes in the thermosetting oven.

Table 3.3: Composition of the SiO₂ NPs respective to the PVA-PAA Solution.

Set	SiO ₂ (wt%)	PVA-PAA (wt%)
1	-	100.0
2	0.1	99.9
3	0.2	99.8
4	0.3	99.7
5	0.4	99.6
6	0.5	99.5

3.6 Characterization of Membrane

Characterization of membrane is very crucial as it provides the overview of the membrane properties. The dried SiO₂ NPs powder was characterized by means of Fourier-Transform Infrared Spectrometer (FTIR) and X-Ray Diffraction (XRD). After the fabrication of PVA-PAA-SiO₂ membrane, the characteristic of the membrane was examined using FTIR and Scanning Electron Microscope (SEM).

3.6.1 X-Ray Diffraction (XRD)

XRD was conducted to investigate the structure of the SiO₂ NPs synthesized according to the diffraction peak. Shimadzu XRD-6000 was used in this study with the scan range between 2° to 80° while the X-ray beam wavelength was selected at 1.5406 Å.

3.6.2 Fourier-Transform Infrared Spectrometer (FTIR)

FTIR was used to identify the functional group and chemical bonds available on the SiO₂ NPs and membrane sample. In this project, Nicolet IS10 FTIR spectrometer was used and the FTIR spectra was measured within 400 to 4000 cm⁻¹. A total of 64 scans were performed to obtain the spectrum at a resolution of 4 cm⁻¹. The FTIR was measured on the SiO₂ NPs, pristine PES membrane and the PVA-PAA-SiO₂ membrane. The presence of the functional group and chemical bonds can be clearly observed with the pristine PES membrane as the reference membrane.

3.6.3 Scanning Electron Microscope (SEM)

SEM (S-3400, Hitachi, Japan) was used to study the surface morphology of the pristine PES membrane and PVA-PAA-SiO₂ coated membrane from the high-resolution images. Prior to the SEM analysis, smaller size of the specimen was obtained from the membrane and coated with gold for 45 seconds in a vacuum chamber. This was to make sure that the samples were sufficiently conductive for the SEM to analyses as the membrane were non-conductive. The SEM was supplied with 15.0 kV and the magnification power was set at x 50.0 k.

3.7 Performance of Membrane

3.7.1 Dead-end Filtration System

A dead-end filtration cell unit with an effective membrane area of 14.6 cm² was used to determine the water permeation flux and rejection performance of the coated membrane (Kamal et al., 2019). As shown in Figure 3.2 the membrane was placed inside the filtration unit containing the feed solution. Next, the feed solution was forced through the membrane using nitrogen gas as an inert gas at

ambient temperature with a constant pressure (Ayaz et al., 2019). Lastly, the permeate passed through the membrane will be collected for further calculation.

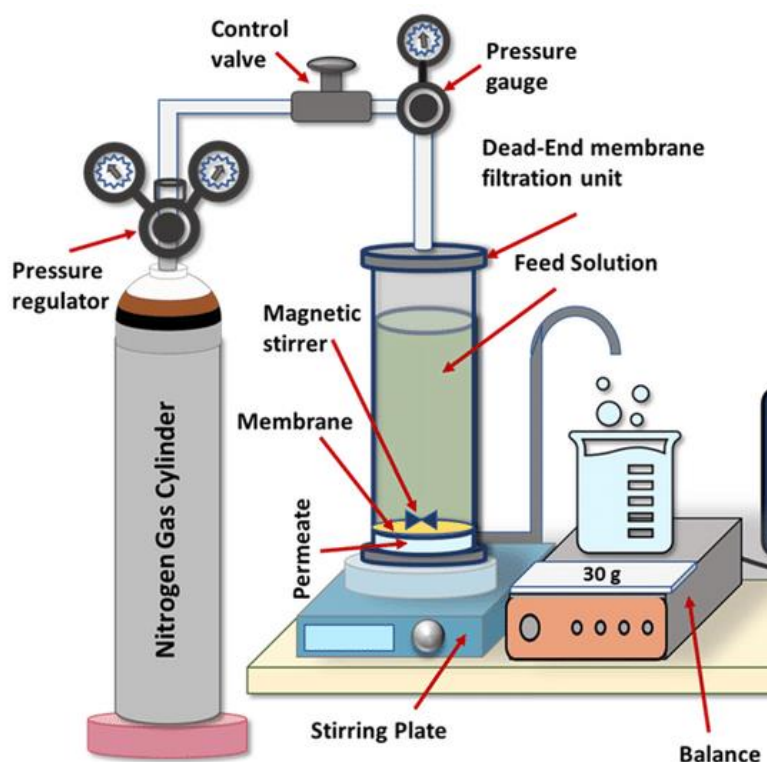


Figure 3.2: Dead-end Filtration Cell Unit (Kamal et al., 2019)

3.7.1.1 Pure Water Flux

In order to investigate the water permeation flux of the membranes, pure water flux was tested on the pristine PES membrane and the PVA-PAA membranes with different SiO₂ NPs loading. Firstly, the membrane was dried before running the water flux test as the moisture content of the membrane would affect the water flux experiment, resulting in inaccurate result. To ensure the membrane could fit properly in the filtration unit, the membrane was cut into a specific shape. After placing the membrane in the filtration unit, the filtration unit was tightly screwed to ensure constant pressure within the system. Next, 150 ml of distilled water was filled in the filtration unit and compaction process was carried out by channelling the nitrogen gas under 4 bars for 20 minutes to ensure the constant water flux. The water flux test was operated at 2 bars and ran for 20 minutes. The following Equation 3.1 was used to calculate the pure water flux (Ayaz et al., 2019).

$$J_w = \frac{Q}{A \times \Delta t} \quad (3.1)$$

where J_w = pure water flux (L/m²h)

Q = volume of permeate collected (L)

A = effective membrane area (m²)

Δt = permeation time (h)

3.7.1.2 Rejection Test

The rejection test was held on pristine PES membrane and PVA-PAA membranes with different SiO₂ NPs loading. The rejection test was conducted with a feed solution containing 10 mg/L of tartrazine dye. The test was operated under 2 bars for 10 minutes. The concentration of the feed solution and the permeate solution were determined using the UV-Vis spectrophotometer with absorbance value at the wavelength of 427 nm. The difference between the concentration of the solution was used to evaluate the rejection performance of the coated membrane. The following equation was used to calculate rejection (Heng et al., 2021).

$$R (\%) = \left(1 - \frac{C_p}{C_F} \right) \times 100 \% \quad (3.2)$$

where R = rejection of solute (%)

C_p = concentration of solute in permeate solution (mg/L)

C_F = concentration of solute in feed solution (mg/L)

3.7.2 Self-Healing Test

Self-healing test was used to determine the capability of the membrane to self-heal by measuring the pure water flux and rejection of the membrane. To make the experiment more precise and consistent, an artificial wound was created on the membrane surface. As seen from Figure 3.3 the membrane's surface was damaged by a pair of blades using standard weight (Kim, Getachew and Kim, 2017). Next, the water flux and rejection of the damaged membrane were

investigated. After that, the self-healing process was performed by immersing the damaged membrane in water for 48 hours. Lastly, the healed membrane was tested again for the water flux and rejection. The self-healing efficiency was calculated using Equation 3.3 (Tan and Tee, 2021).

$$\eta = \frac{J_w \text{ healed} - J_w \text{ damage}}{J_w \text{ pristine} - J_w \text{ damage}} \times 100\% \quad (3.3)$$

where J_w = pure water flux (L/m^2h)

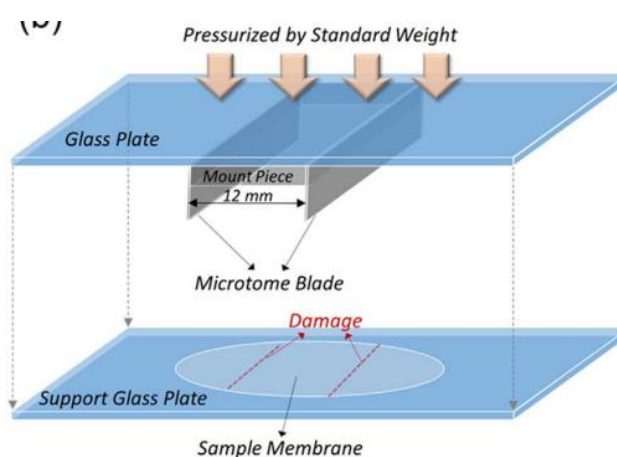


Figure 3.3: Introduce Artificial Damage to the Membrane's Surface (Kim, Getachew and Kim, 2017).

3.7.3 Stability Test

The stability of the PVA-PAA-SiO₂ membrane can be evaluated in terms of water flux and dye rejection performance over the target duration immersing in water. The PVA-PAA-SiO₂ membrane was immersed in the distilled water at room temperature for 2 weeks. After 2 weeks of immersion, the membrane was removed from the water and let dry in room temperature before performing the pure water flux test and dye rejection (Zhu et al., 2018).

3.7.4 Mechanical Properties

The tensile test was carried out to determine the tensile strength and elongation at break using the universal tensile tester with a load cell rated for a maximum load of 50 N and a precision of 0.001 N. Tensile strength refers to the maximum stress that a material can endure when subjected to pull apart with specific load. Elongation at break refers to the ability of the material to resist deformation before rupture. The membrane samples were cut into 9 cm in length and 1 cm in width using a blade. The thickness of the membrane was measured using the micrometre screw gauge. The samples were measured with a gauge length of 15 mm while the tensile rate maintained at 20 mm/min. All the measurements were obtained for the membrane samples with different SiO₂ NPs loading.

CHAPTER 4

RESULTS AND DISCUSSION

4.1 Characterization of Membrane

4.1.1 X-Ray Diffraction (XRD) Analysis

The findings from X-ray Diffraction (XRD) analysis as depicted in Figure 4.1 were utilized to ascertain the crystalline configuration of the synthesized SiO₂ NPs. Tran et al. (2013) reported that the typical broad peak centered at 22.5° is attributed to the amorphous phase of the SiO₂ NPs. The broad XRD reflection peak observed could be attributed to the small dimensions and incomplete internal structure of the synthesized particles, indicating that a significant proportion of these particles exhibit an amorphous nature (Dubey, Rajesh and More, 2015). A study by Sldozian (2014) revealed that, despite the general belief that crystalline structure is more stable than the amorphous state, producing SiO₂ NPs in the amorphous state is preferable due to its higher activity compared to crystalline silica. This is because amorphous silica has higher mechanical properties and a higher quality in the non-destructive test. Besides, as no additional impurity peaks were observed, indicating the purity of the SiO₂ NPs.

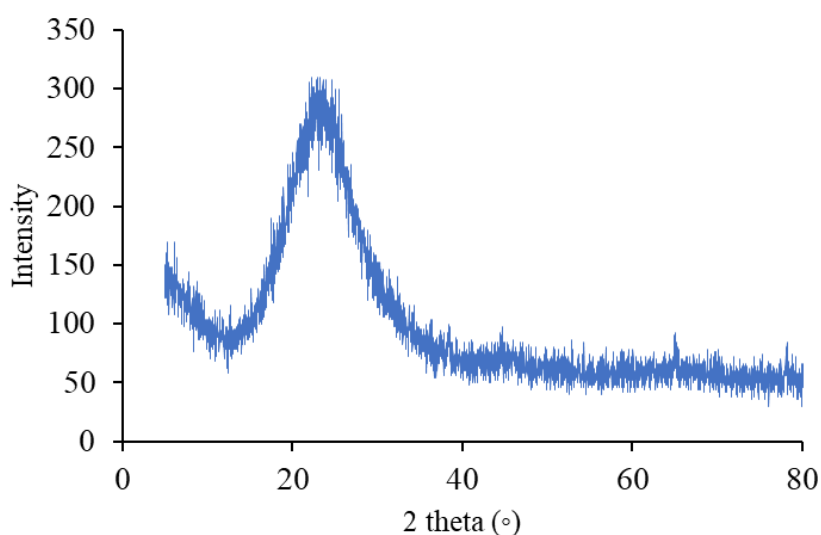


Figure 4.1: XRD Patterns for SiO₂ NPs.

4.1.2 Fourier Transform Infrared (FTIR) Analysis

The synthesized SiO₂ NPs and fabricated membrane were analysed with the FTIR to assess the functional group presence in the sample. Figure 4.2 depicts the FTIR spectra of the SiO₂ NPs, PVA-PAA membrane and PVA-PAA-SiO₂ membrane, respectively. As shown from Figure 4.2, the vibration peaks at 450.30 cm⁻¹, 804.17 cm⁻¹ and 1065 cm⁻¹ belong to the bending mode of SiO₂, symmetric and asymmetric stretching of Si-O-Si, respectively. These peaks show the chemical structure of the SiO₂, confirming the successful synthesis of the nanoparticles.

Besides, referring to the FTIR spectrum of PVA-PAA in Figure 4.2(b), the broad peak at the 3369.03 cm⁻¹ and the sharp peak at 1103.57 cm⁻¹ correspond to the O-H stretching and C-O stretching of the PVA and PAA, respectively while the stretching vibration peak of C=O at 1720.67 cm⁻¹ indicates the esterification of the PVA and PAA (Song et al., 2014). The C-O-C ester vibration peak at 1071.26 cm⁻¹ further support the esterification reaction between the cross-linking of PVA and PAA (Kim et al., 2019). With the inclusion of the SiO₂ NPs, it was noticeable from Figure 4.2(c) that the wavenumber of C=O slightly increases from 1720.67 to 1730 cm⁻¹ which indicates to the condensation reaction of the COOH group of PAA and OH group of SiO₂. This could be attributed to the cleavage of C=O bond, forming the covalent linkage, resulting in a decrease in mass and subsequently causing an increase in vibration frequency and wavenumber (Heng et al., 2021). Moreover, the presence of the SiO₂ NPs is evident from the pronounced peaks at 1089.1 cm⁻¹ represents the Si-O-Si asymmetric vibrations, 949.29 cm⁻¹ signifies the Si-OH vibration, and 795.97 cm⁻¹ denotes the Si-O stretching (Kim et al., 2019).

Regarding the hydroxyl group, in comparing the PVA-PAA membrane with PVA-PAA-SiO₂ membrane in Figure 4.2(b) and (c), respectively, the O-H stretching vibration band became broader at the wavenumber of 3369.03 cm⁻¹ and 3367.59 cm⁻¹, respectively. It indicated a decrease in hydroxyl groups as the SiO₂ NPs formed hydrogen bonding in the membrane.

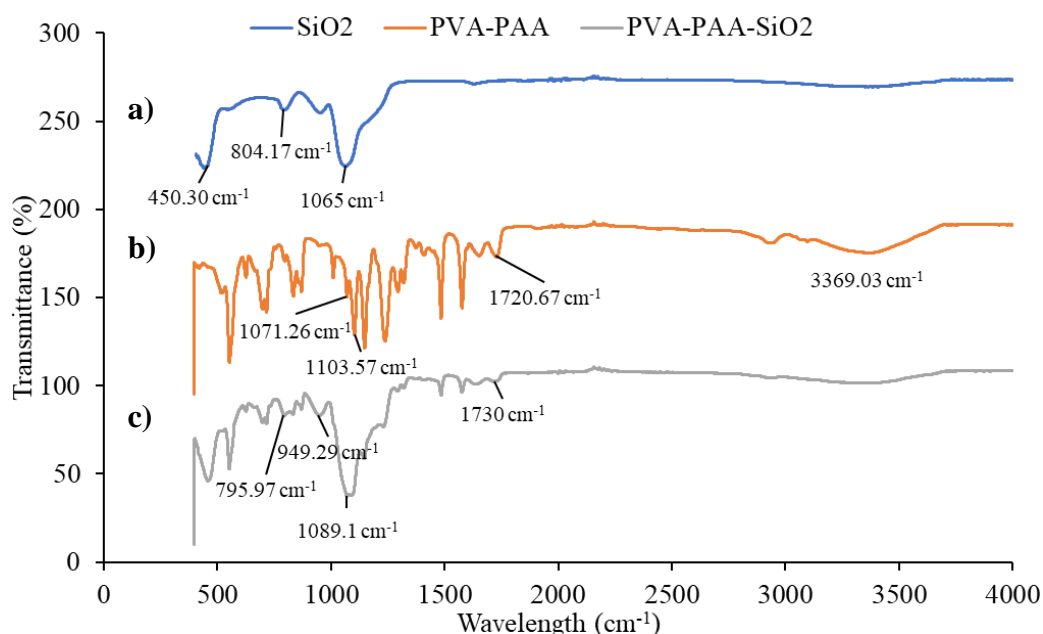


Figure 4.2: FTIR Spectra of (a) SiO₂ NPs; (b) PVA-PAA Membrane and (c) PVA-PAA-SiO₂ Membrane.

4.1.3 Scanning Electron Microscopy (SEM) Analysis

The surface morphologies on the top surface of the membrane were observed through the SEM images. The pure PVA-PAA membrane in Figure 4.3(a) exhibits a uniform surface morphology and the SiO₂ NP was evenly distributed within the PVA-PAA composite membrane for Figure 4.3(b-f). It is noteworthy that the membranes with SiO₂ NPs loading of 0.1 wt% and 0.2 wt% as depicted in Figure 4.3(b) and (c), respectively, have smoother surface. However, increasing the SiO₂ NPs loading results in significant changes of the surface morphology, where obvious protruding particles can be observed from the membrane surfaces as shown in Figure 4.3(d). As depicted from Figure 4.3(e) and (f), the elevated concentration of additives within the polymer solution caused the SiO₂ NPs to be irregularly distributed throughout the membrane surface. This uneven arrangement of nanoparticles contributed to the formation of a dense membrane surface. As the amount of SiO₂ NPs increase, it tends to aggregate and agglomerate, resulting in a broad range of particle sizes which would reduce the pore size of the membrane affecting the permeability.

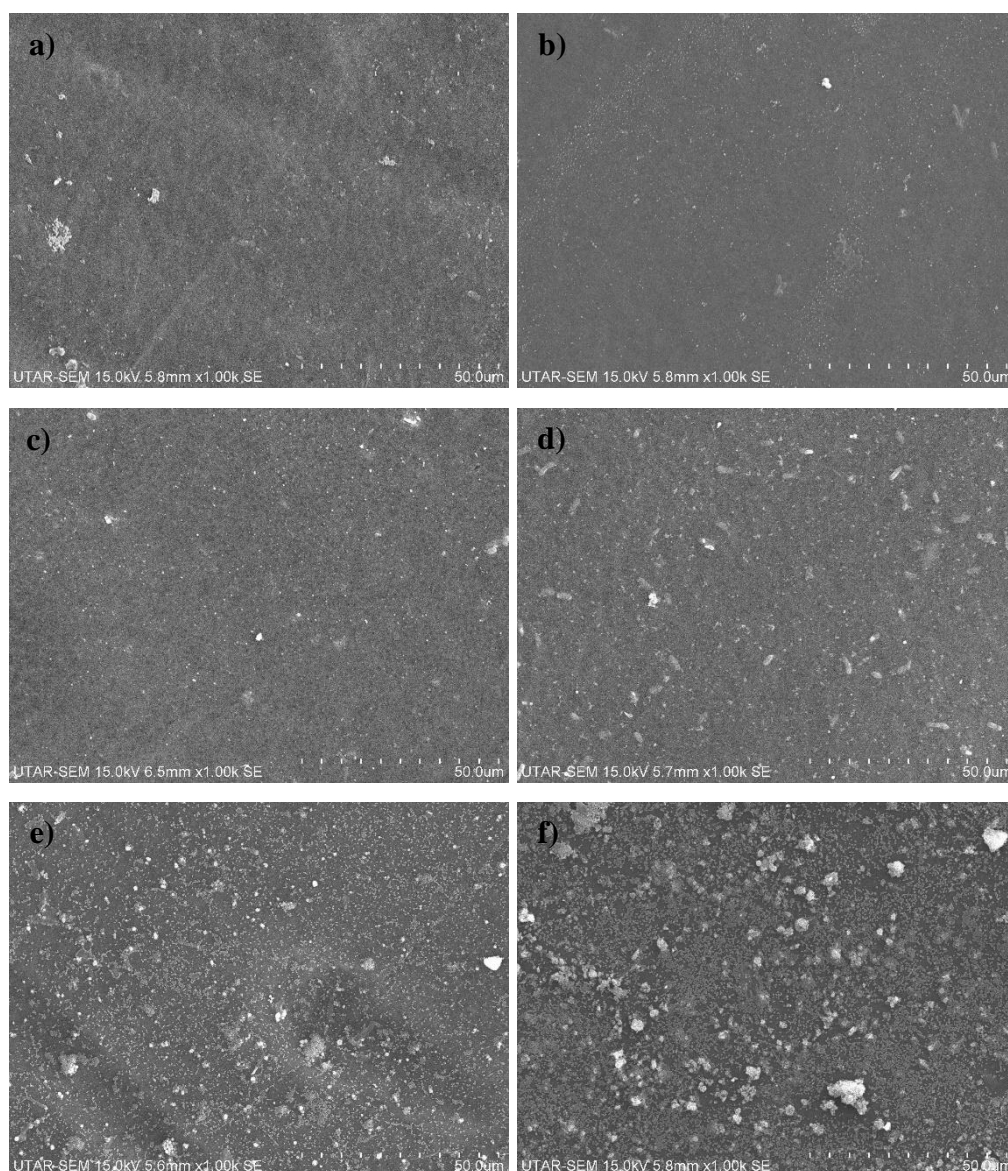


Figure 4.3: Top-View SEM Images of membrane with (a) pure PVA-PAA; (b) 0.1 wt% SiO₂ loading; (c) 0.2 wt% SiO₂ loading; (d) 0.3 wt% SiO₂ loading; (e) 0.4 wt% SiO₂ loading and (f) 0.5 wt% SiO₂ loading.

4.2 Performance of Membrane

4.2.1 Membrane Permeation Flux

The effect of SiO₂ NPs loading on the water permeation flux of the membrane is illustrated in Figure 4.4. The addition of SiO₂ NPs resulted in a great improvement in water flux performance as compared to the pure PVA-PAA membrane. However, the water flux decreased upon the optimal inclusion of the SiO₂ NPs. As shown in Figure 4.4, the water permeation flux increased from 36.16 L/m²h to 53.84 L/m²h when the SiO₂ NPs loading increased from 0 to 0.3

wt%. To elucidate, the pure water flux of the PVA-PAA membrane inclined with the loading of SiO₂ NP as it contained large amount of hydroxyl group on its surface which contributed to the hydrophilicity of the membrane. Additionally, the PVA-PAA structure and the SiO₂ NPs were bonded by the hydrogen bond which also increases the hydrophilicity of the membrane and draws more water molecules towards the membrane. On the other hand, further increment of the SiO₂ NPs caused the agglomeration of the nanoparticles on the membrane surface, increasing the surface roughness and reducing pore size, results in the declining water permeation flux (Liu, Jiang and Li, 2023). This can be linked from the SEM analysis as shown in Figure 4.3(e) and (f) where the 0.4 wt% and 0.5 wt% SiO₂ NPs were clumped together affecting the pore size. Although higher concentration of SiO₂ NPs increases the hydroxyl group but it was claimed that will affect pore size which had greater influence on the water flux performance (Liu, Jiang and Li, 2023).

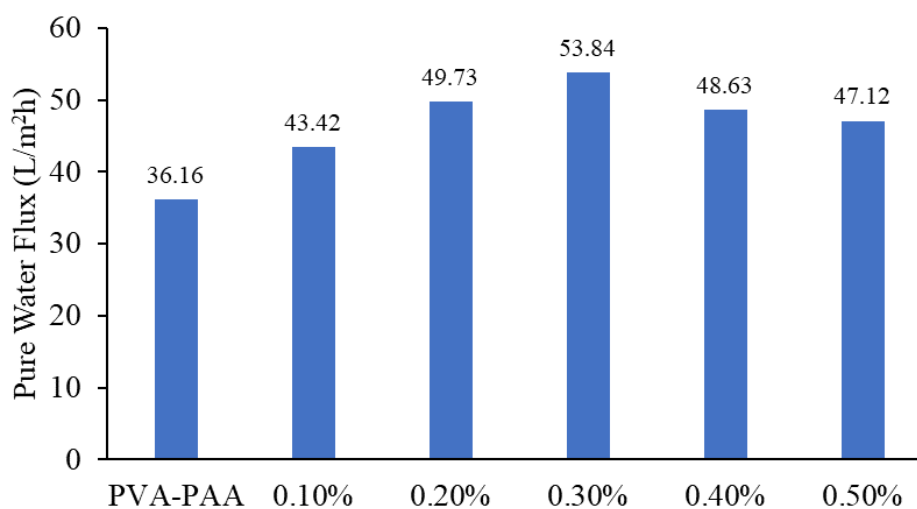


Figure 4.4: Water Flux of PVA-PAA Membrane with Different SiO₂ NPs Loading.

4.2.2 Self-Healing Test

As the membrane are subjected to damage during the operation in real life application, the self-healing ability was investigated. The self-healing test was studied on the coated membrane with different SiO₂ NPs loading and the finding was demonstrated in Figure 4.5. It can be noticed that the healing efficiency of the membrane shows an increasing trend with the SiO₂ NPs loading and decline after the optimum point. For damaged PVA-PAA membrane, the pure water flux increased from 36.16 L/m²h to 65.21 L/m²h and gradually decreased to 47.12 L/m²h after immersing in water for 24 hours. This phenomenon demonstrates the healing performance of the water-responsive membrane. Furthermore, the PVA-PAA membrane with 0.3 wt% SiO₂ NPs loading showed the highest healing efficiency of 73.05% as compared to pristine PVA-PAA membrane that show 62.26% healing efficiency. The healing mechanism of the PVA-PAA was due to the reversible hydrogen bond between the free hydroxyl group and the water molecule. With the inclusion of SiO₂ NPs, it increases the mobile hydroxyl group that could form multiple hydrogen bond at the scratch interfaces (Jucius, Lazauskas and Gudaitis, 2019).

Moreover, it can be noticed that the pure water flux of each membrane after healed will be relatively higher than the initial reading. This might be due to the filling of the damage area with the OH hydrophilic group during the self-healing process (Liu, Jiang and Li, 2023). When the membrane experiences physical damage, the self-healing mechanism occurs through the swelling and molecular diffusion of the functional group. Consequently, the membrane after healed exhibited higher hydrophilicity.

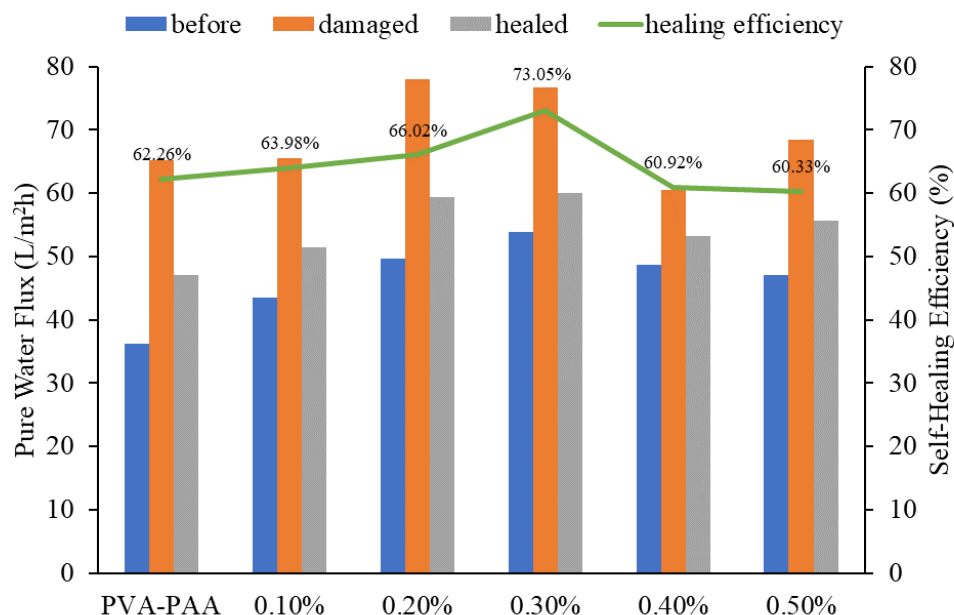


Figure 4.5: Self-Healing Efficiency of PVA-PAA Membrane with Different SiO₂ NPs Loading.

Since 0.3 wt% of SiO₂ NPs loading membrane exhibited the highest healing performance, it was further studied on the effect of timescale as shown in Figure 4.6. It can be noticed that the membrane coated with SiO₂ NPs recovered better from 71.43% to 90.29% after 48 hours of immersion in water and eventually reached its reheel limit upon longer time.

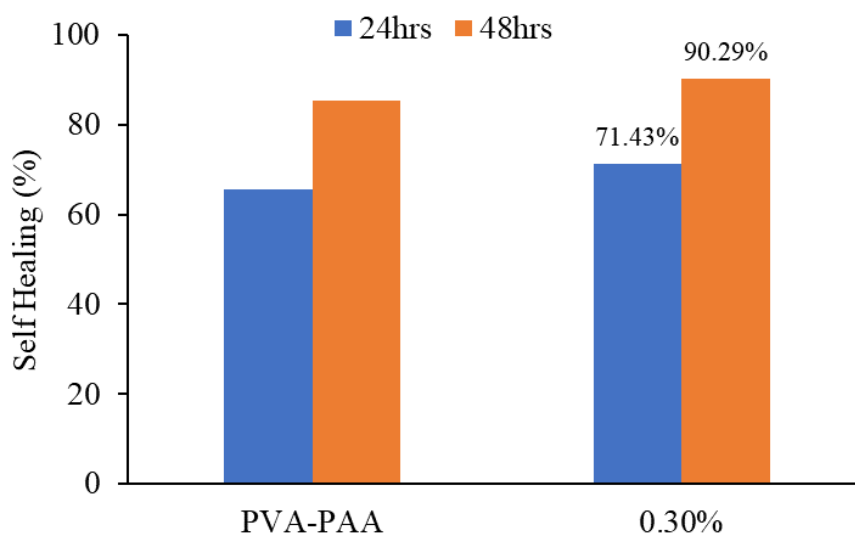


Figure 4.6: Self-Healing Efficiency of PVA-PAA Membrane with Different Healing Period.

To further examine the healing behaviour of the membrane, top surface morphology of the membrane was studied using SEM. Figure 4.7 depicts the SEM images of PVA-PAA-SiO₂ membrane after damaged and after healed, respectively. As observed from the images, after sustaining physical damage, the membrane demonstrated the capability to fill and heal the affected areas. This ability was facilitated by the swelling characteristics of the polymer and restoration of damaged and fractured polymer chain (Liu, Jiang and Li, 2023).

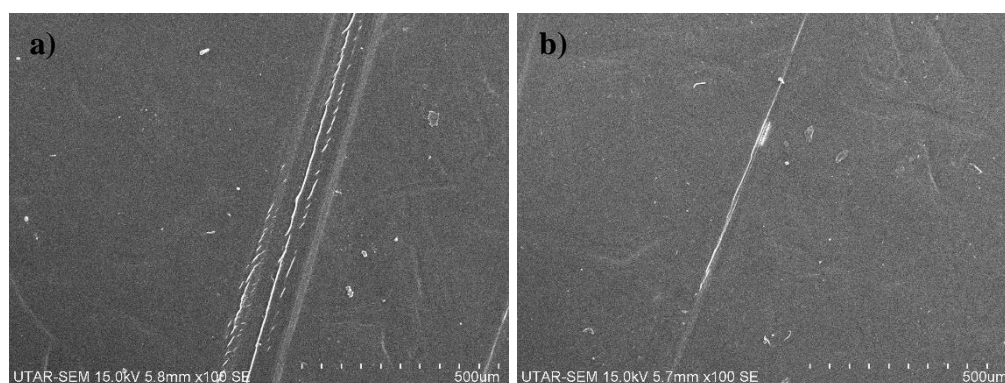


Figure 4.7: Top-View SEM Images of SiO₂ Membrane with (a) Scratch on the Surface and (b) After Immersed in Water for 48 hours.

4.2.3 Membrane Rejection Test

The rejection performance of the prepared membrane with 0.3 wt% SiO₂ NPs loading towards the tartrazine dye is shown in Figure 4.8. As for the PVA-PAA membrane, the rejection before damage, after damaged and after healed was 24.87%, 4.91% and 10.12%, respectively, whereas for the membrane with 0.3 wt% SiO₂ NP was 59.13%, 12.82% and 34.42%, respectively. The PVA-PAA membrane with 0.3 wt% SiO₂ NPs loading had a rejection rate that was noticeably higher than the pristine PVA-PAA membrane as the NPs having an anion charge that influences the degree of sorption of the dye. To elucidate, the pristine PVA-PAA membrane fabricated was originally negatively charge on the surface while the negatively charge SiO₂ NPs further increase the electronegativity of the composite. The heightened presence of hydrophilic oxygen-containing group (hydroxyl) on the surface of SiO₂ NPs is responsible for this phenomenon (Gai, Zhao and Chung, 2018). Moreover, the tartrazine dye

carried a negatively charged which results in electrostatic repulsion between the membrane and the dye, which enhanced the rejection.

Apart from that, the rejection of dye is also affected by the pore size of the membrane which is due to the steric hindrance effect. The membrane containing 0.3 wt% SiO₂ NPs exhibited superior retention due to the addition of NP, which facilitated the formation of a denser membrane internal structure, thereby enhancing the interception of dye molecules (Liu, Jiang and Li, 2023).

Besides, it can be noticed that the rejection of tartrazine dye was the highest before damage and largely reduced after experiencing damage. The primary cause of the decline in the tartrazine rejection is due to the breakage of the membrane structure, resulting in reduced density and hindered the interception of dye molecule (Yang et al., 2023). Although the membrane's rejection can be retained after immersed in water for 24 hours but it could not revert to the original performance as some of the dye molecule has stained on the damage site affecting the healing process.

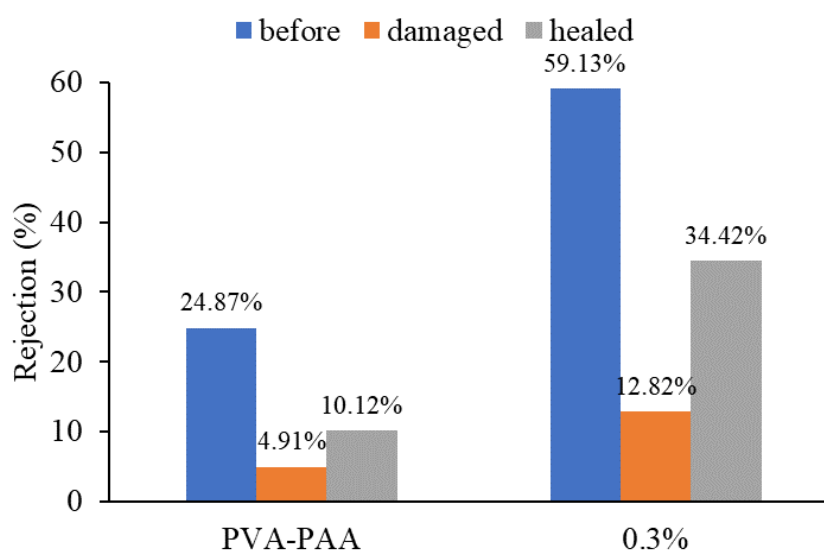


Figure 4.8: Rejection Performance of Membrane at Different State.

4.2.4 Stability Test

Another criteria that has been studied is the stability of the membrane performance after immersing in water for 2 weeks. As mentioned earlier, the PVA-PAA membrane tends to dissolve in water which affect the long-term application in the wastewater industry, therefore, SiO₂ NPs was added into the PVA-PAA membrane to examine its effect towards the solubility of the modified membrane. Figure 4.9 depicts the effect of water flux performance after immersed in water. In detail, the water flux of the PVA-PAA membrane increased from 36.16 L/m²h to 92.88 L/m²h while PVA-PAA-SiO₂ membrane had a stable water flux of 53.84 L/m²h to 52.33 L/m²h after immersing in water for 2 weeks. The high water flux of the PVA-PAA membrane is due to the dissolution of the polymer chain into the water, causing a bigger membrane pore on the PES membrane surface. Conversely, the membrane embraced with SiO₂ NPs exhibited a consistent water flux performance, indicating that the polymer chain is highly resistant to dissolution in water. In essence, the level of interaction between SiO₂ NPs and the water molecules is not substantial enough to surpass the strong and extensive covalent bonds between silicon and oxygen atom. Consequently, the membrane remained its performance even after the immersion in water.

Furthermore, the rejection performance was illustrated in Figure 4.9. It can be observed that the tartrazine rejection of the pristine membrane decreased from 23.71% to 13.40%. This indicates that the polymer chain of PVA-PAA dissolve in water forming a loosen structure that fails to trap the dye molecules during the filtration process. This aligns with the challenges encountered in the water treatment plant. On the other hand, the PVA-PAA membrane coated with SiO₂ NPs demonstrated a stable tartrazine rejection of 55.98% to 54.08% even after the membrane was immersed in water for 2 weeks. This shows that the membrane has the ability to maintain its structural integrity and performance over time even when exposed to water.

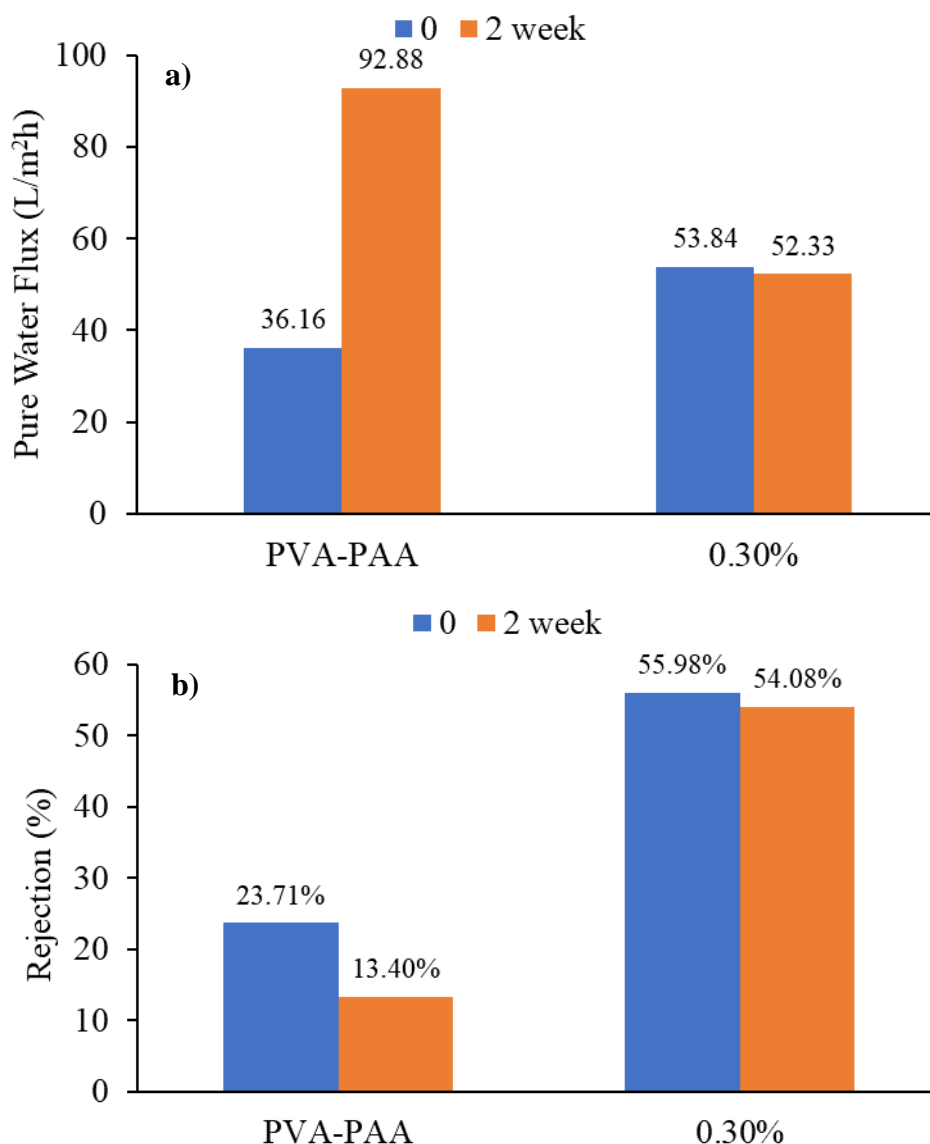


Figure 4.9: Performance of Membrane over Time in terms of (a) Pure Water Flux and (b) Dye Rejection.

4.2.5 Mechanical Properties

In general, the mechanical characteristics of the membrane are typically linked to the spatial configuration of the polymer, attributes of the polymer blend component and the bonds among the polymer. The stress-strain curve of the membrane with different SiO₂ NPs loading was displayed in Figure 4.10. The tensile strength of the membrane increased from 6.45 MPa to 11.41 MPa and reduced to 4.85 MPa with incorporation of 0 wt%, 0.3 wt% and 0.5 wt% of NPs, respectively. Besides, the elongation of the PVA-PAA membrane incorporated with different SiO₂ NPs loading was 119.38%, 138.73% and 72.64% at 0 wt%,

0.3 wt% and 0.5 wt% of NPs, respectively. These findings all pointed to the possibility that the membrane may become mechanically stronger by the addition of 0.3 wt% SiO₂ NPs in PVA-PAA membrane revealing the highest level of mechanical properties. It has been demonstrated that adding NPs to the PVA-PAA membrane increases the elasticity and tensile modulus. The main causes of the results were the stiffness of SiO₂ NPs and the polymer entanglement brought about by the contact between the membrane and the SiO₂ NPs, which strengthen the membrane's mechanical characteristics. To elucidate, the incorporated SiO₂ NPs will penetrate the pore crevices of the membrane thereby diminishing the pore size and tightening the structure of the membrane which will led to heighten the physical resistance of the membrane (Widiyandari et al., 2021). In contrast, the 0.5 wt% SiO₂ NPs in the PVA-PAA membrane shown a decreasing performance in both the tensile strength and elongation due to the severe agglomeration of NP above the critical level and causes the non-uniformity of the membrane structure (Ashraf et al., 2018). In other word, the non-uniform compact network leads to less chain mobility and less free volume which reduces the elongation at break of the film.

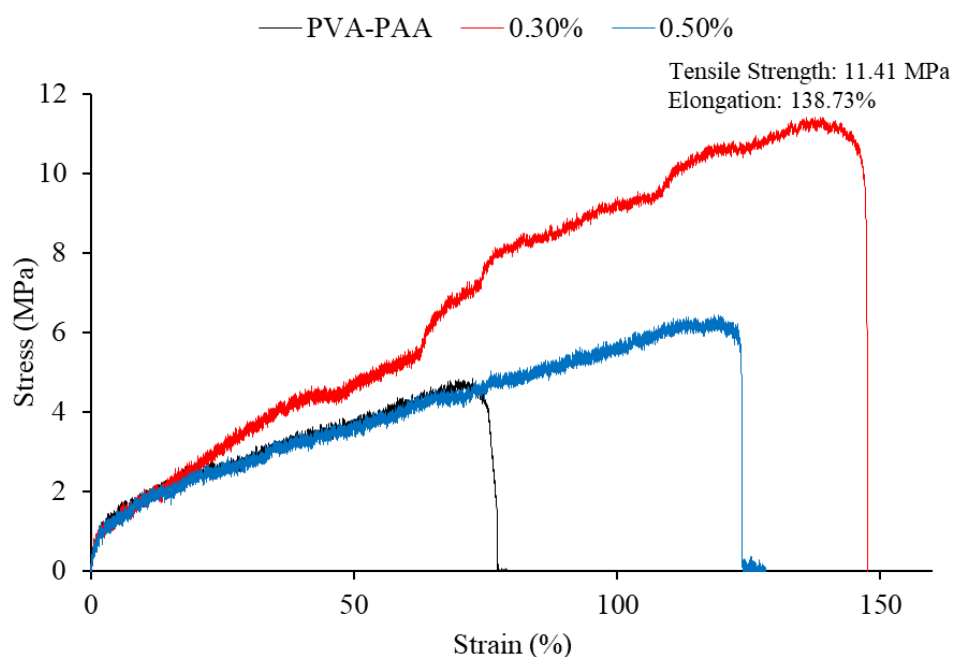


Figure 4.10: Stress-Strain Curve of the PVA-PAA Membrane with Different SiO₂ NPs Loading.

CHAPTER 5

CONCLUSIONS AND RECOMMENDATIONS

5.1 Conclusions

To encapsulate the work, the SiO₂ NPs was successfully synthesized through the Stöber method. The characterization of SiO₂ NPs preceded the experimental phase, involving FTIR and XRD analysis. The FTIR analysis revealed the presence of SiO₂ NPs with the functional group of Si-O-Si at different vibration peak. Besides, the XRD analysis demonstrated that the SiO₂ NPs exhibited an amorphous structure, which significantly contributed to its high stability and activity.

A pristine PVA-PAA membrane and a series of SiO₂ NPs with different dosages of 0.1, 0.2, 0.3, 0.4 and 0.5 wt% were prepared and characterized using FTIR and SEM. The FTIR results shown the condensation reaction between the COOH group of the PAA and OH group of SiO₂ NPs indicating the successful fabrication of PVA-PAA-SiO₂ membrane. The presence of SiO₂ NPs in the PVA-PAA membrane affects the membrane morphology as shown in the SEM images. PVA-PAA membrane with 0.3 wt% SiO₂ NPs had depicted obvious protruding particles on the surface. Excessive addition of SiO₂ NPs had led to uneven distribution of nanoparticles resulted in dense membrane surface.

Furthermore, the effect of the SiO₂ NPs on the self-healing efficiency of the PVA-PAA membrane was evaluated. The optimal nanoparticles loading in the PVA-PAA polymer composite was determined to be 0.3 wt% based on the experiment results. Under the conditions of optimal nanoparticles loading, a pure water flux of 53.84 L/m²h and self-healing efficiency of 71.43% and 90.29% were achieved after immersing in water for 24 hours and 48 hours, respectively. Also, the rejection performance of the membrane was tested with tartrazine dye. The 0.3 wt% SiO₂ NPs membrane demonstrated better rejection of 59.13% than the pristine PVA-PAA membrane which was only 24.87%. It also shown that the rejection could retained back to 34.42 % after damage was introduced.

Lastly, the PVA-PAA membrane stability with the addition of SiO₂ NPs were studied. Through a comprehensive analysis of various composition of PVA-PAA-SiO₂, several key findings have emerged. The stability of the

membrane incorporated with 0.3 wt% of SiO₂ NPs in terms of water flux and rejection were consistent after immersing in water for 2 weeks. The tensile strength and elongation of the PVA-PAA membrane with 0.3 wt% SiO₂ NPs was 11.41 MPa and 138.73%, respectively, which were higher than the pure PVA-PAA membrane. All the finding suggested that the addition of 0.3 wt% of SiO₂ NPs in the PVA-PAA membrane exhibited the best performance.

5.2 Recommendations

The experiment was executed successfully in accordance with the predetermined objectives and scopes. Several suggestions could be considered to enhance the future research endeavours, aiming for a more comprehensive outcome.

1. Additional parameters can be study to achieve the optimal performance of the membrane. For example, the casting conditions such as speed and temperature will affect the membrane structure while the composition of polymer blend will affect the membrane properties.
2. Modification on nanoparticles functional group can tailor the membrane properties to facilitate in specific applications. In the study of Kim et al. (2019), thiol group was added to the nanoparticles to enhance the adsorption performance.
3. Advanced characterization analysis should be carried out to gain deeper insights into the membrane surface properties for instances the zeta potential to study the surface charge of the membrane, water contact angle to determine the hydrophilicity of the membrane.
4. Further scale-up studies should be carried out to evaluate the feasibility of manufacturing membrane on a large scale for practical applications.
5. Longer stability test should be carried out by extending the test to more weeks or month.

REFERENCES

- Agboola, O., Fayomi, O.S.I., Ayodeji, A., Ayeni, A.O., Alagbe, E.E., Sanni, S.E., Okoro, E.E., Moropeng, L., Sadiku, R., Kupolati, K.W. and Oni, B.A., 2021. A Review on Polymer Nanocomposites and Their Effective Applications in Membranes and Adsorbents for Water Treatment and Gas Separation. *Membranes*, 11(2), p.139.
- Asad, A., Sameoto, D. and Sadrzadeh, M., 2020. Overview of membrane technology. In: *Nanocomposite Membranes for Water and Gas Separation*. Elsevier. pp.1–28.
- Ashraf, M.A., Peng, W., Zare, Y. and Rhee, K.Y., 2018. Effects of Size and Aggregation/Agglomeration of Nanoparticles on the Interfacial/Interphase Properties and Tensile Strength of Polymer Nanocomposites. *Nanoscale Research Letters*, 13(1), p.214.
- Ayaz, M., Muhammad, A., Younas, M., Khan, A.L. and Rezakazemi, M., 2019. Enhanced Water Flux by Fabrication of Polysulfone/Alumina Nanocomposite Membrane for Copper(II) Removal. *Macromolecular Research*, 27(6), pp.565–571.
- Boonmahitthisud, A., Nakajima, L., Nguyen, K.D. and Kobayashi, T., 2017. Composite effect of silica nanoparticle on the mechanical properties of cellulose-based hydrogels derived from cottonseed hulls. *Journal of Applied Polymer Science*, 134(10).
- Bouarroudj, T., Aoudjit, L., Djahida, L., Zaidi, B., Ouraghi, M., Zioui, D., Mahidine, S., Shekhar, C. and Bachari, K., 2021. Photodegradation of tartrazine dye favored by natural sunlight on pure and (Ce, Ag) co-doped ZnO catalysts. *Water Science and Technology*, 83(9), pp.2118–2134.
- Burcu Altin, 2009. *Synthesis and Characterization of Monodisperse Silica Based Functional Nanoparticles for Multi-Purpose Applications*.
- Chen, X., Dam, M.A., Ono, K., Mal, A., Shen, H., Nutt, S.R., Sheran, K. and Wudl, F., 2002. A Thermally Re-mendable Cross-Linked Polymeric Material. *Science*, 295(5560), pp.1698–1702.
- Cordier, P., Tournilhac, F., Soulié-Ziakovic, C. and Leibler, L., 2008. Self-healing and thermoreversible rubber from supramolecular assembly. *Nature*, 451(7181), pp.977–980.
- Dannert, C., Stokke, B.T. and Dias, R.S., 2019. Nanoparticle-Hydrogel Composites: From Molecular Interactions to Macroscopic Behavior. *Polymers*, 11(2), p.275.
- David Richard Steinmetz, 2007. *Texture Evolution in Processing of Polystyrene-Clay Nanocomposites*.

- Dubey, R.S., Rajesh, Y.B.R.D. and More, M.A., 2015. Synthesis and Characterization of SiO₂ Nanoparticles via Sol-gel Method for Industrial Applications. *Materials Today: Proceedings*, 2(4–5), pp.3575–3579.
- Findik, F., 2021. Nanomaterials and their applications. *Periodicals of Engineering and Natural Sciences*, 9(3), pp.62–75.
- Gai, W., Zhao, D.L. and Chung, T.-S., 2018. Novel thin film composite hollow fiber membranes incorporated with carbon quantum dots for osmotic power generation. *Journal of Membrane Science*, 551, pp.94–102.
- Getachew, B.A., Kim, S.-R. and Kim, J.-H., 2017. Self-Healing Hydrogel Pore-Filled Water Filtration Membranes. *Environmental Science & Technology*, 51(2), pp.905–913.
- Ghosh, P., Singh Rana, S., Kumar C, S., Chandra Pradhan, R. and Mishra, S., 2015. Membrane filtration of fruit juice - An emerging technology. *International Journal of Food and Nutritional Sciences*, 4(4), pp.47–57.
- Guillen, G.R., Pan, Y., Li, M. and Hoek, E.M. V., 2011. Preparation and Characterization of Membranes Formed by Nonsolvent Induced Phase Separation: A Review. *Industrial & Engineering Chemistry Research*, 50(7), pp.3798–3817.
- Gürses, A., Güneş, K. and Şahin, E., 2021. Removal of dyes and pigments from industrial effluents. In: *Green Chemistry and Water Remediation: Research and Applications*. Elsevier. pp.135–187.
- Haraguchi, K., Takehisa, T. and Fan, S., 2002. Effects of Clay Content on the Properties of Nanocomposite Hydrogels Composed of Poly(*N* - isopropylacrylamide) and Clay. *Macromolecules*, 35(27), pp.10162–10171.
- Heng, Z.W., Tan, Y.Y., Chong, W.C., Mahmoudi, E., Mohammad, A.W., Teoh, H.C., Sim, L.C. and Koo, C.H., 2021. Preparation of a novel polysulfone membrane by incorporated with carbon dots grafted silica from rice husk for dye removal. *Journal of Water Process Engineering*, 40, p.101805.
- Huang, C.-H. and Liu, Y.-L., 2017. Self-healing polymeric materials for membrane separation: an example of a polybenzimidazole-based membrane for pervaporation dehydration on isopropanol aqueous solution. *RSC Advances*, 7(61), pp.38360–38366.
- Huang, L., Zhao, S., Wang, Z., Wu, J., Wang, J. and Wang, S., 2016. In situ immobilization of silver nanoparticles for improving permeability, antifouling and anti-bacterial properties of ultrafiltration membrane. *Journal of Membrane Science*, 499, pp.269–281.
- Huisman, I.H., 2000. MEMBRANE SEPARATIONS | Microfiltration. In: *Encyclopedia of Separation Science*. Elsevier. pp.1764–1777.

- Jucius, Lazauskas and Gudaitis, 2019. Multiple Hydrogen-Bonding Assisted Scratch-Healing of Transparent Coatings. *Coatings*, 9(12), p.796.
- Kamal, N., Kochkodan, V., Zekri, A. and Ahzi, S., 2019. Polysulfone Membranes Embedded with Halloysite Nanotubes: Preparation and Properties. *Membranes*, 10(1), p.2.
- Khan, I., Saeed, K. and Khan, I., 2019. Nanoparticles: Properties, applications and toxicities. *Arabian Journal of Chemistry*, 12(7), pp.908–931.
- Khraisheh, M., Elhenawy, S., AlMomani, F., Al-Ghouti, M., Hassan, M.K. and Hameed, B.H., 2021. Recent Progress on Nanomaterial-Based Membranes for Water Treatment. *Membranes*, 11(12), p.995.
- Kim, J., Kang, T., Kim, H., Shin, H.J. and Oh, S.-G., 2019. Preparation of PVA/PAA nanofibers containing thiol-modified silica particles by electrospinning as an eco-friendly Cu (II) adsorbent. *Journal of Industrial and Engineering Chemistry*, 77, pp.273–279.
- Kim, S.-R., Getachew, B.A. and Kim, J.-H., 2017. Toward microvascular network-embedded self-healing membranes. *Journal of Membrane Science*, 531, pp.94–102.
- Kononova, S. V., Kremnev, R. V., Gubanova, G.N., Vlasova, E.N., Popova, E.N., Vylegzhanina, M.E. and Volkov, A.Ya., 2022. Effect of Phase Heterogeneity on the Properties of Poly(vinyl alcohol)-Based Composite Pervaporation Membranes. *Membranes*, 12(12), p.1185.
- Li, F. and Xia, H., 2017. Dopamine-functionalized poly(vinyl alcohol) elastomer with melt processability and self-healing properties. *Journal of Applied Polymer Science*, 134(28).
- Li, L. and Hsieh, Y.-L., 2005. Ultra-fine polyelectrolyte hydrogel fibres from poly(acrylic acid)/poly(vinyl alcohol). *Nanotechnology*, 16(12), pp.2852–2860.
- Lim, Y.H., Wong, E.C., Chong, W.C., Mohammad, A.W., Koo, C.H. and Lau, W.J., 2024. Introducing self-healing properties to polyethersulfone (PES) membrane via poly(vinyl alcohol)/ polyacrylic acid (PVA/PAA) surface coating. *Chemosphere*, 349, p.140772.
- Limin, W. and Baghdachi, J., 2015. *Functional Polymer Coatings*. Hoboken, NJ: John Wiley & Sons, Inc.
- Lin, W., Zhu, T., Li, Q., Yi, S. and Li, Y., 2012. Study of pervaporation for dehydration of caprolactam through PVA/nano silica composite membranes. *Desalination*, 285, pp.39–45.
- Liu, S., Fang, F., Wu, J. and Zhang, K., 2015. The anti-biofouling properties of thin-film composite nanofiltration membranes grafted with biogenic silver nanoparticles. *Desalination*, 375, pp.121–128.

- Liu, S., Jiang, H. and Li, Y., 2023. Construction of tight ultrafiltration membrane for efficient dye/salt separation with physical and chemical self-healing property. *Chemical Engineering Journal*, 467, p.143456.
- Liu, S., Rao, Z., Wu, R., Sun, Z., Yuan, Z., Bai, L., Wang, W., Yang, H. and Chen, H., 2019a. Fabrication of Microcapsules by the Combination of Biomass Porous Carbon and Polydopamine for Dual Self-Healing Hydrogels. *Journal of Agricultural and Food Chemistry*, 67(4), pp.1061–1071.
- Liu, Y., Zhang, K., Sun, J., Yuan, J., Yang, Z., Gao, C. and Wu, Y., 2019b. A Type of Hydrogen Bond Cross-Linked Silicone Rubber with the Thermal-Induced Self-Healing Properties Based on the Nonisocyanate Reaction. *Industrial & Engineering Chemistry Research*, 58(47), pp.21452–21458.
- Liu, Y.-L. and Chuo, T.-W., 2013. Self-healing polymers based on thermally reversible Diels–Alder chemistry. *Polymer Chemistry*, 4(7), p.2194.
- Lu, H., Wang, J., Stoller, M., Wang, T., Bao, Y. and Hao, H., 2016. An Overview of Nanomaterials for Water and Wastewater Treatment. *Advances in Materials Science and Engineering*, 2016, pp.1–10.
- M. Ways, T.M., Ng, K.W., Lau, W.M. and Khutoryanskiy, V. V., 2020. Silica Nanoparticles in Transmucosal Drug Delivery. *Pharmaceutics*, 12(8), p.751.
- Market and Research, 2019. *Membrane Filtration Market - Types, Applications (Water, Dairy, Drinks & Concentrates, Wine & Beer), Module Design, Membrane Materials and Regional Global Outlook*.
- Mezzomo, L., Ferrara, C., Brugnetti, G., Callegari, D., Quartarone, E., Mustarelli, P. and Ruffo, R., 2020a. Exploiting Self-Healing in Lithium Batteries: Strategies for Next-Generation Energy Storage Devices. *Advanced Energy Materials*, 10(46), p.2002815.
- Mezzomo, L., Ferrara, C., Brugnetti, G., Callegari, D., Quartarone, E., Mustarelli, P. and Ruffo, R., 2020b. Exploiting Self-Healing in Lithium Batteries: Strategies for Next-Generation Energy Storage Devices. *Advanced Energy Materials*, 10(46), p.2002815.
- Modrzejewska, Z., Dorabialska, M., Zarzycki, R. and Wojtasz-Pająk, A., 2009. The Mechanism of Sorption of Ag⁺ Ions on Chitosan Microgranules. *Progress on Chemistry and Application of Chitin and its Derivatives*, 14, pp.49–64.
- Nadtoka, O., Kutsevol, N., Bezugla, T., Virych, P. and Naumenko, A., 2020. Hydrogel-Silver Nanoparticle Composites for Biomedical Applications. *Ukrainian Journal of Physics*, 65(5), p.446.
- Nakum, J. and Bhattacharya, D., 2022. Various Green Nanomaterials Used for Wastewater and Soil Treatment: A Mini-Review. *Frontiers in Environmental Science*, 9.

- Ngang, H.P., Ahmad, A.L., Low, S.C. and Ooi, B.S., 2017. Preparation of PVDF/SiO₂ composite membrane for salty oil emulsion separation: Physicochemical properties changes and its impact on fouling propensity. *IOP Conference Series: Materials Science and Engineering*, 206, p.012083.
- Paralikar, S.A., Simonsen, J. and Lombardi, J., 2008. Poly(vinyl alcohol)/cellulose nanocrystal barrier membranes. *Journal of Membrane Science*, 320(1–2), pp.248–258.
- Precedence Research, 2023. *Membrane Filtration Market (By Type: Reverse osmosis (RO), Ultrafiltration (UF), Microfiltration (MF), Nanofiltration (NF))*.
- Rami Joseph Aghajan Sldozian, 2014. Comparison between the properties of Amorphous and Crystalline - Nano SiO₂ additives on Concrete. *International Journal of Scientific & Engineering Research*, 5(6), pp.1437–1443.
- Richard W, B., 2004. *Membrane Technology and Applications*. 2nd ed. John Wiley & Sons Ltd.
- Selim, A., Toth, A.J., Fozer, D., Haaz, E. and Mizsey, P., 2020. Pervaporative desalination of concentrated brine solution employing crosslinked PVA/silicate nanoclay membranes. *Chemical Engineering Research and Design*, 155, pp.229–238.
- Shao, C., Wang, M., Chang, H., Xu, F. and Yang, J., 2017. A Self-Healing Cellulose Nanocrystal-Poly(ethylene glycol) Nanocomposite Hydrogel via Diels–Alder Click Reaction. *ACS Sustainable Chemistry & Engineering*, 5(7), pp.6167–6174.
- Shawky, H.A., Yasin, R., Kotp, Y.H. and Eissa, D., 2020. Biosynthesis of silver nanoparticles and its effect on TFC RO membrane for groundwater desalination. *DESALINATION AND WATER TREATMENT*, 193, pp.34–47.
- Shehata, N., Egirani, D., Olabi, A.G., Inayat, A., Abdelkareem, M.A., Chae, K.-J. and Sayed, E.T., 2023. Membrane-based water and wastewater treatment technologies: Issues, current trends, challenges, and role in achieving sustainable development goals, and circular economy. *Chemosphere*, 320, p.137993.
- Shemer, H., Wald, S. and Semiat, R., 2023. Challenges and Solutions for Global Water Scarcity. *Membranes*, 13(6), p.612.
- Singh, R., 2006. *Hybrid Membrane Systems for Water Purification: Technology, Systems Design and Operations*. 1st ed. Elsevier Science & Technology Books.
- Song, J., Zhou, M., Yi, R., Xu, T., Gordin, M.L., Tang, D., Yu, Z., Regula, M. and Wang, D., 2014. Interpenetrated Gel Polymer Binder for High-Performance Silicon Anodes in Lithium-ion Batteries. *Advanced Functional Materials*, 24(37), pp.5904–5910.

- Spoljaric, S., Salminen, A., Dang Luong, N., Lahtinen, P., Vartiainen, J., Tammelin, T. and Seppälä, J., 2014a. Nanofibrillated cellulose, poly(vinyl alcohol), montmorillonite clay hybrid nanocomposites with superior barrier and thermomechanical properties. *Polymer Composites*, 35(6), pp.1117–1131.
- Spoljaric, S., Salminen, A., Dang Luong, N., Lahtinen, P., Vartiainen, J., Tammelin, T. and Seppälä, J., 2014b. Nanofibrillated cellulose, poly(vinyl alcohol), montmorillonite clay hybrid nanocomposites with superior barrier and thermomechanical properties. *Polymer Composites*, 35(6), pp.1117–1131.
- Suhas, D.P., Aminabhavi, T.M., Jeong, H.M. and Raghu, A. V., 2015. Hydrogen peroxide treated graphene as an effective nanosheet filler for separation application. *RSC Advances*, 5(122), pp.100984–100995.
- Tan, Y.J. and Tee, B.C.K., 2021. *Recent Trends in Self-Healing Soft Electronic Materials and Devices*. Material Matters.
- Tran, T.N., Anh Pham, T. Van, Phung Le, M.L., Thoa Nguyen, T.P. and Tran, V.M., 2013. Synthesis of amorphous silica and sulfonic acid functionalized silica used as reinforced phase for polymer electrolyte membrane. *Advances in Natural Sciences: Nanoscience and Nanotechnology*, 4(4), p.045007.
- Utrera-Barrios, S., Verdejo, R., López-Manchado, M.A. and Hernández Santana, M., 2020. Evolution of self-healing elastomers, from extrinsic to combined intrinsic mechanisms: a review. *Materials Horizons*, 7(11), pp.2882–2902.
- Wang, Y., Shi, Y., Gu, Y., Xue, P. and Xu, X., 2021. Self-Healing and Highly Stretchable Hydrogel for Interfacial Compatible Flexible Paper-Based Micro-Supercapacitor. *Materials*, 14(8), p.1852.
- Wei, Z., Yang, J.H., Du, X.J., Xu, F., Zrinyi, M., Osada, Y., Li, F. and Chen, Y.M., 2013. Dextran-Based Self-Healing Hydrogels Formed by Reversible Diels–Alder Reaction under Physiological Conditions. *Macromolecular Rapid Communications*, 34(18), pp.1464–1470.
- White, S.R., Sottos, N.R., Geubelle, P.H., Moore, J.S., Kessler, M.R., Sriram, S.R., Brown, E.N. and Viswanathan, S., 2001. Autonomic healing of polymer composites. *Nature*, 409(6822), pp.794–797.
- Widiyandari, H., Putra, O.A., Purwanto, A. and Subagio, A., 2021. Fabrication of PVDF/SiO₂ Nanofiber Membrane as A Separator of Li-ion Battery by Double Jet Sprayers Electrospinning Method. *IOP Conference Series: Materials Science and Engineering*, 1096(1), p.012142.
- Xiao, W., Jiang, X., Liu, X., Zhou, W., Garba, Z.N., Lawan, I., Wang, L. and Yuan, Z., 2021. Adsorption of organic dyes from wastewater by metal-doped porous carbon materials. *Journal of Cleaner Production*, 284, p.124773.
- Xing, W. and Tang, Y., 2022. On mechanical properties of nanocomposite hydrogels: Searching for superior properties. *Nano Materials Science*, 4(2), pp.83–96.

- Xu, C., Nie, J., Wu, W., Zheng, Z. and Chen, Y., 2019. Self-Healable, Recyclable, and Strengthened Epoxidized Natural Rubber/Carboxymethyl Chitosan Biobased Composites with Hydrogen Bonding Supramolecular Hybrid Networks. *ACS Sustainable Chemistry & Engineering*, 7(18), pp.15778–15789.
- Xu, P., Shang, Z., Yao, M. and Li, X., 2022. Mechanistic insight into improving strength and stability of hydrogels via nano-silica. *Journal of Molecular Liquids*, 357, p.119094.
- Yang, Q., Zhang, L., Xie, X., Sun, Q., Feng, J., Dong, H., Song, N., Yu, L. and Dong, L., 2023. Self-healing polyamide reverse osmosis membranes with temperature-responsive intelligent nanocontainers for chlorine resistance. *Frontiers of Chemical Science and Engineering*, 17(9), pp.1183–1195.
- Yin, J., Yang, Y., Hu, Z. and Deng, B., 2013. Attachment of silver nanoparticles (AgNPs) onto thin-film composite (TFC) membranes through covalent bonding to reduce membrane biofouling. *Journal of Membrane Science*, 441, pp.73–82.
- Yue, H., Wang, Z. and Zhen, Y., 2022. Recent Advances of Self-Healing Electronic Materials Applied in Organic Field-Effect Transistors. *ACS Omega*, 7(22), pp.18197–18205.
- Zaidi, S., Fadhilah, F., Saleem, H., Hawari, A. and Benamor, A., 2019. Organically Modified Nanoclay Filled Thin-Film Nanocomposite Membranes for Reverse Osmosis Application. *Materials*, 12(22), p.3803.
- Zhang, T., Zheng, W., Wang, Q., Wu, Z. and Wang, Z., 2023. Designed strategies of nanofiltration technology for Mg²⁺/Li⁺ separation from salt-lake brine: A comprehensive review. *Desalination*, 546, p.116205.
- Zhu, M., Hua, D., Pan, H., Wang, F., Manshian, B., Soenen, S.J., Xiong, R. and Huang, C., 2018. Green electrospun and crosslinked poly(vinyl alcohol)/poly(acrylic acid) composite membranes for antibacterial effective air filtration. *Journal of Colloid and Interface Science*, 511, pp.411–423.
- Zhuravlev, L.T., 2000. The surface chemistry of amorphous silica. Zhuravlev model. *Physicochemical and Engineering Aspects*, pp.1–38.